Article

Cell

Multi-invasions Are Recombination Byproducts that Induce Chromosomal Rearrangements

Graphical Abstract

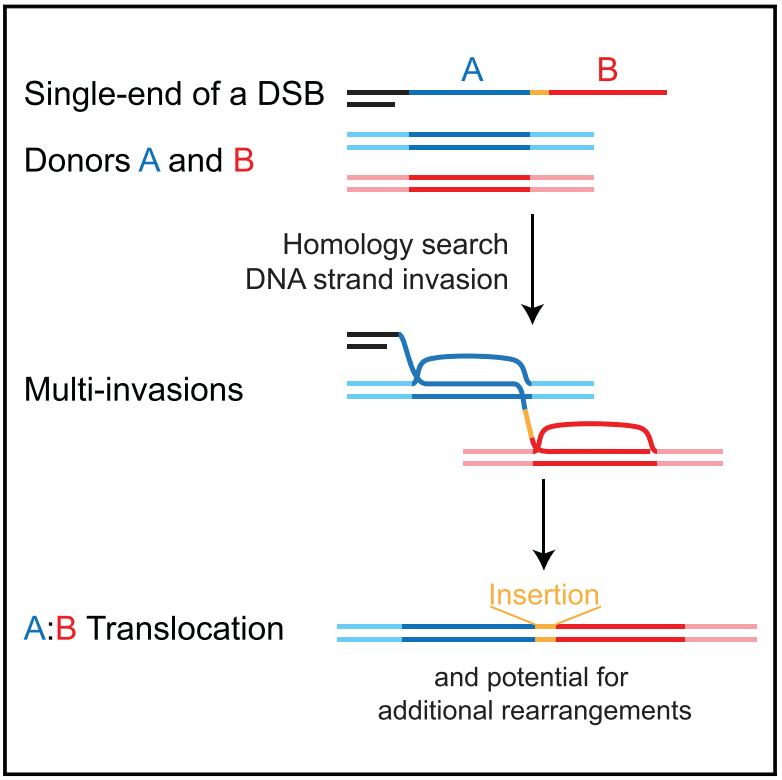

Authors

Aurèle Piazza, William Douglass Wright, Wolf-Dietrich Heyer

Correspondence

wdheyer@ucdavis.edu

In Brief

Translocation between two intact chromosomes can be induced by an independent lesion on a third chromosome.

Highlights

- MIs are HR intermediates formed when one ssDNA invades more than one dsDNA donor
- MIs cause rearrangement of intact donors with flush translocation junctions and insertions
- Endonucleases promote, and D-loop disruption restricts, MI-induced rearrangements
- MI-induced rearrangements propagate secondary DSBs causing further rearrangements

Piazza et al., 2017, Cell *170*, 760–773
August 10, 2017 © 2017 Elsevier Inc.
http://dx.doi.org/10.1016/j.cell.2017.06.052

CellPress

Cell

Article

Multi-invasions Are Recombination Byproducts that Induce Chromosomal Rearrangements

Aurèle Piazza,[1] William Douglass Wright,[1] and Wolf-Dietrich Heyer[1,2,3,*]
[1]Department of Microbiology and Molecular Genetics, One Shields Avenue, University of California, Davis, Davis, CA 95616, USA
[2]Department of Molecular and Cellular Biology, One Shields Avenue, University of California, Davis, Davis, CA 95616, USA
[3]Lead Contact
*Correspondence: wdheyer@ucdavis.edu
http://dx.doi.org/10.1016/j.cell.2017.06.052

SUMMARY

Inaccurate repair of broken chromosomes generates structural variants that can fuel evolution and inflict pathology. We describe a novel rearrangement mechanism in which translocation between intact chromosomes is induced by a lesion on a third chromosome. This multi-invasion-induced rearrangement (MIR) stems from a homologous recombination byproduct, where a broken DNA end simultaneously invades two intact donors. No homology is required between the donors, and the intervening sequence from the invading molecule is inserted at the translocation site. MIR is stimulated by increasing homology length and spatial proximity of the donors and depends on the overlapping activities of the structure-selective endonucleases Mus81-Mms4, Slx1-Slx4, and Yen1. Conversely, the 3′-flap nuclease Rad1-Rad10 and enzymes known to disrupt recombination intermediates (Sgs1-Top3-Rmi1, Srs2, and Mph1) inhibit MIR. Resolution of MIR intermediates propagates secondary chromosome breaks that frequently cause additional rearrangements. MIR features have implications for the formation of simple and complex rearrangements underlying human pathologies.

INTRODUCTION

Maintenance of genomic stability depends on the ability to both prevent formation of DNA damage and to repair damage faithfully. Accurate repair of DNA double-strand breaks (DSBs) is paramount to avoid structural alterations of the genome. Homologous recombination (HR) repairs DSBs with high fidelity using an intact homologous donor sequence as a template. Yet, multiple mutant contexts have revealed that deregulated HR is prone to generate both chromosomal rearrangements (Kolodner et al., 2002) and toxic intermediates that threaten cellular viability (Fabre et al., 2002; Gangloff et al., 2000). Thus, the formidable accuracy of HR is not only an intrinsic property of the core HR machinery but is further enforced by a battery of regulatory activities that reverse intermediates of the pathway prior to final product formation (reviewed in Heyer, 2015).

A crucial step of HR is the search for homology performed by a heterotypic nucleoprotein filament composed of the single-stranded DNA (ssDNA) flanking the DSB site coated with the prototypical RecA-family recombinase (Rad51 in eukaryotes) and associated proteins (Bell and Kowalczykowski, 2016). A combination of in vitro and in vivo single molecule studies provided key insights into the long-lasting conundrum of homology search (Bell and Kowalczykowski, 2016). First, the increased mobility of the broken molecule promotes exploration of the nuclear volume (Dion et al., 2012; Miné-Hattab and Rothstein, 2012). Second, the multivalent nature of the RecA/Rad51-ssDNA filament exploits the several hundreds to thousands of nucleotides exposed by resection (Symington, 2016) to simultaneously sample multiple double-stranded DNA (dsDNA), in a model referred to as intersegmental contact sampling (Forget and Kowalczykowski, 2012). This search mechanism predicts that, if homology is present on different molecules, one filament may invade (i.e., form heteroduplex DNA within) multiple donors simultaneously. In agreement with this prediction, we uncovered multi-invasion (MI) intermediates in reconstituted in vitro reactions with ssDNA mimicking physiological resection products (Wright and Heyer, 2014).

Here, we investigate the potential threat to genomic stability posed by the MI byproduct of homology search during HR. We uncovered multi-invasion-induced rearrangements (MIR) wherein two intact dsDNA molecules are translocated upon invasion by a third, broken molecule. We outline its requirements, regulation, consequences for genomic stability, and discuss implications of MIR features for simple and complex rearrangements in other organisms.

RESULTS

One ssDNA Molecule Can Form MI with Yeast and Human Recombination Proteins In Vitro

Using a reconstituted homologous DNA pairing reaction, we previously showed that Rad51 and Rad54 proteins can form higher order joint DNA molecules in addition to the primary, single displacement loop (D-loop) (Wright and Heyer, 2014). We interpreted these species as being heteroduplex DNA formed in multiple dsDNA molecules by a single ssDNA. We named these new D-loop intermediates multiple invasions (MIs) (Wright and Heyer, 2014). Here, we sought to formally demonstrate the nature of these joint DNA molecule species.

First, we performed D-loop reactions using a substrate with 98 bp 5′ and 1,201 nt ssDNA (ds98-*1201*) (Wright and Heyer,

2014) homologous to donor plasmids of two different sizes (A, A*), which allows electrophoretic differentiation of each D-loop species (Figure 1A). While each donor gives rise to a specific pattern of single (1°) and MIs (2° and 3°), addition of both donors produces a unique species corresponding to the simultaneous invasion of the A and A* donors in addition to the sum of the two independent profiles (Figure 1A, left). The presence of both donors in the A+A* MI product was corroborated by Southern blotting using donor-specific probes (Figure 1A, right). Thus, these results demonstrate that the slower migrating joint molecules are MIs, which account for ~30% of D-loop products. Formation of MIs is not a consequence of the limited pairing length (≈200 nt) permitted by the number of supercoils in our standard donor plasmid, as they also form with a linear dsDNA donor devoid of such topological constraint (Figure S1A). Further, to demonstrate that one molecule of ssDNA can tether two non-related donor sequences, we generated substrates bearing ~400 nt-long regions of homology to donors A and B (Figure S1B). While addition of either the A or B donor mainly gives rise to a single invasion, simultaneous addition of both donors produces a discrete MI band with supercoiled plasmid (Figures S1B and S1C) or linear dsDNA donors (Figure S1D). Terminal 5′ and 3′ heterologies do not prevent MI formation (Figure S1C). Quantification reveals that MIs are equal to the product of the independent single invasions (Figures 1A and S1D). These results demonstrate that MIs do not form sequentially at the 3′ end, but that invasions can occur internally and independently from one another.

Yeast Rad51 has distinct biochemical features compared to human RAD51 (Bugreev and Mazin, 2004). Therefore, whether human RAD51 and RAD54 proteins could produce MIs was an open question. Using the ds98-*1201* substrate in combination with the A and A* donors, MIs are formed by the human RAD51 and RAD54 proteins (Figure 1B). Time course analysis revealed that the MI species accumulate with delayed kinetics relative to the primary, single D-loop species, to reach ~17% of the total invasions (Figure 1C). Interestingly, the migration pattern of the MI species is slightly different from those generated with yeast proteins, possibly reflecting different shaped branched DNA molecules in the MI products.

MIs are a newly recognized product of homologous recombination that we demonstrate here with yeast and human Rad51/Rad54. This byproduct of homology search and heteroduplex joint formation tethers together two intact dsDNA donors in a multi-branched intermediate (Figure 1D).

Induction of Translocation between Two Donor Loci Initiated by a DSB at a Third Locus

These biochemical findings open the possibility that a DSB may lead to recombination between two unbroken donor molecules. To address this possibility, we designed a genetic assay in diploid *S. cerevisiae* (Figure 2A). A heterozygous DSB-inducible construct replaces the *URA3* locus on chromosome V (chrV). The searching molecule is assumed by a "YS" sequence (the central portion of the *LYS2* gene, hereafter referred to as YS or YS1000-1000) that is present on only one side of the DSB-inducible site (HOcs). This YS sequence bears ~1 kb of homology to two donors ("LY" and "S2") that do not share homology with each other. In our reference strain, these donors replace the *LYS2* gene on each chrII homolog in an allelic configuration referred as to "inter-chromosomal". Translocation of the two donors restores a functional *LYS2* gene, resulting in lysine prototrophy (Lys^+ cell). The basal and induced Lys^+ frequencies are determined for each liquid culture by plating cells onto selective media prior and 2 hr after DSB induction (Figure S2A), when >99% of the molecules are cut (Figure 2B). The basal translocation (Lys^+) frequency of $\sim 3 \times 10^{-7}$ is independent of the presence of the HO gene (Figure S2B). DSB induction stimulates the translocation frequency by two orders of magnitude to 3.1×10^{-5} (Figures 2C and S2B). Formation of the translocation depends on (1) overlapping homology between the searching molecule and both donors (Figure 2E), (2) the presence of both donors (Figure 2E), and (3) a functional HR pathway (Rad51, Rad52, and Rad54) (Figure 2D). Translocation formation is independent of the key non-homologous end joining (NHEJ) factor Dnl4 (Wilson et al., 1997) and is only modestly affected by loss of Pol32, a Polδ subunit required for extensive DNA displacement synthesis that is essential for break-induced replication (BIR) (Lydeard et al., 2007) (Figure 2D). In all cases, the translocants had restored the *LYS2* gene in place of either the LY or the S2 donors on chrII and had repaired the DSB by gene conversion off the intact chrV (see below). These results demonstrate the existence of an HR-dependent mechanism that rearranges two initially intact chromosomes upon DSB induction in a third chromosome.

Sequence Insertion from the Invading Molecule at the Translocation Junction

Interestingly, the translocation does not require homology between the two translocating donors, as LY and S2 do not share homology. To address whether the translocation results from the exact blunt rejoining of the donors or, instead, inserts sequence from the invading ssDNA, we generated a strain bearing a truncated LY donor lacking 200 bp of the 3′ extremity (LY-Δ200bp). The only source of information for this missing sequence is on the broken molecule. This strain exhibits a translocation frequency near identical to the reference LY strain (Figure 2F), demonstrating that the intervening sequence from the broken molecule is inserted at the translocation junction. We conclude that MI-induced rearrangements represent a potential mechanism to generate insertions.

A Single Broken DNA Molecule Causes Translocation of Two Intact Chromosomes

As cells undergoing DSB repair by HR are mainly in the S/G2 phase of the cell cycle (Barlow et al., 2008), translocations likely result from cells bearing two Rad51-ssDNAs upon DSB induction. Two sets of experiments were conducted to address whether a single ssDNA molecule is sufficient to cause donor translocation.

First, we induced DSB formation in G1-arrested cells (STAR Methods). The translocation frequency obtained upon DSB induction in G1-arrested cells was not significantly different from asynchronous cells (Figure 3A). The overall lower Lys^+ frequency in this strain compared to wild-type was attributable

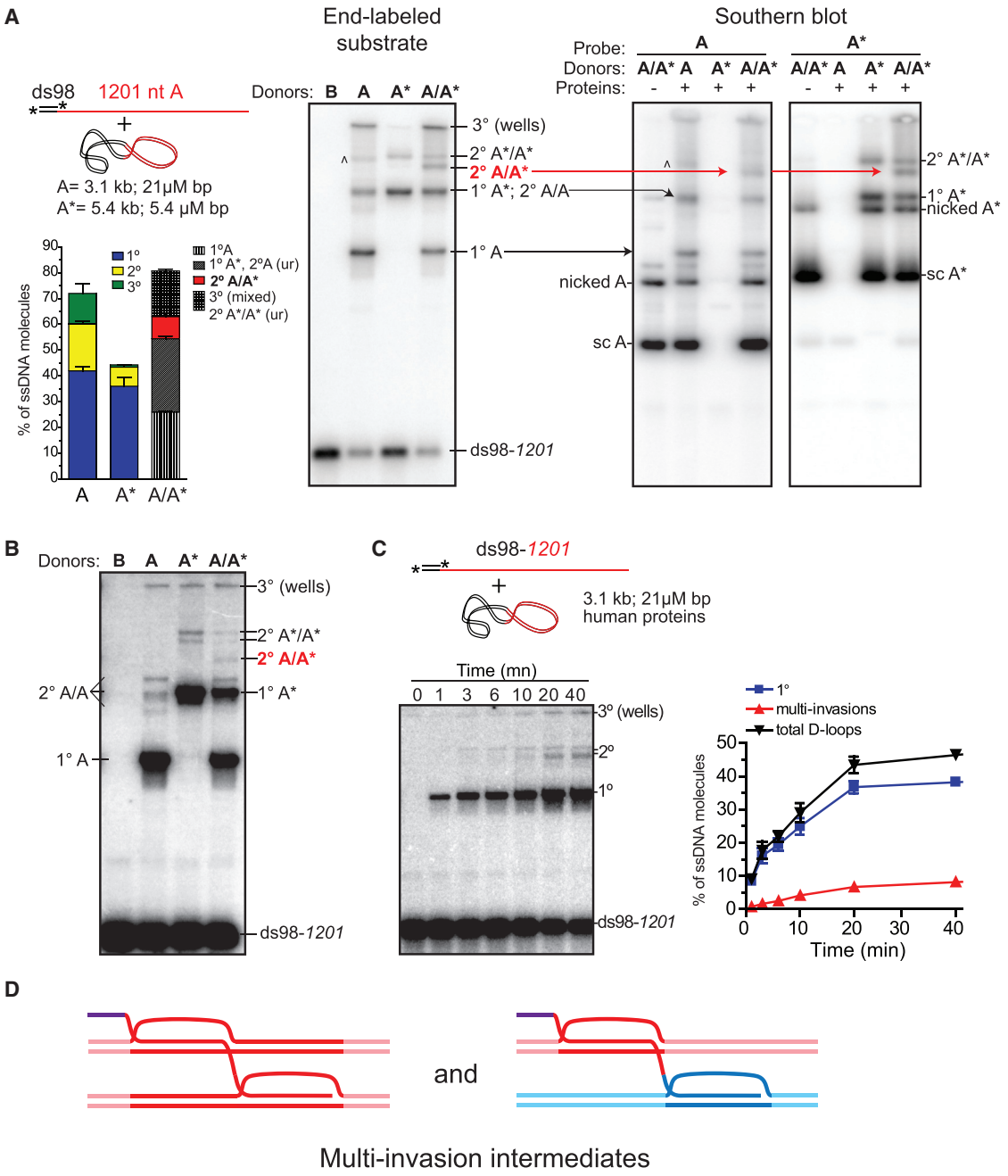

Figure 1. Multi-invasions Form in Reconstituted D-Loop Reactions with Yeast and Human Proteins

(A) D-loop reactions with yeast proteins. A ds98-*1201* (1.3 μM nt/bp; 1 nM molecules) substrate was paired with two different-sized dsDNA plasmids to distinguish multi-invasion (MI) products. Left: ds98-*1201* end-labeled reaction. The main product band is a single D-loop (1°), the next band is 2° (MI: 2 dsDNAs), and the species in the well (3°) likely contains three dsDNAs. A minor product band (^) is likely a 3° invasion species with less complex shape and thus able to enter the gel. Right: Southern blot of D-loop reactions using A- or A*-specific probes. Arrows indicate the corresponding species identified with labeled ssDNA (right) or probing for the plasmid donors (left).

(B) D-loop reactions with human proteins. Reaction conditions (except buffer composition) and analysis as in (A).

(C) Time course with ds98-*1201* substrate using the single donor A. Quantifications in (A) and (C) show the mean ± SD of n = 3.

(D) Scheme of MI joint molecules.

See also Figure S1.

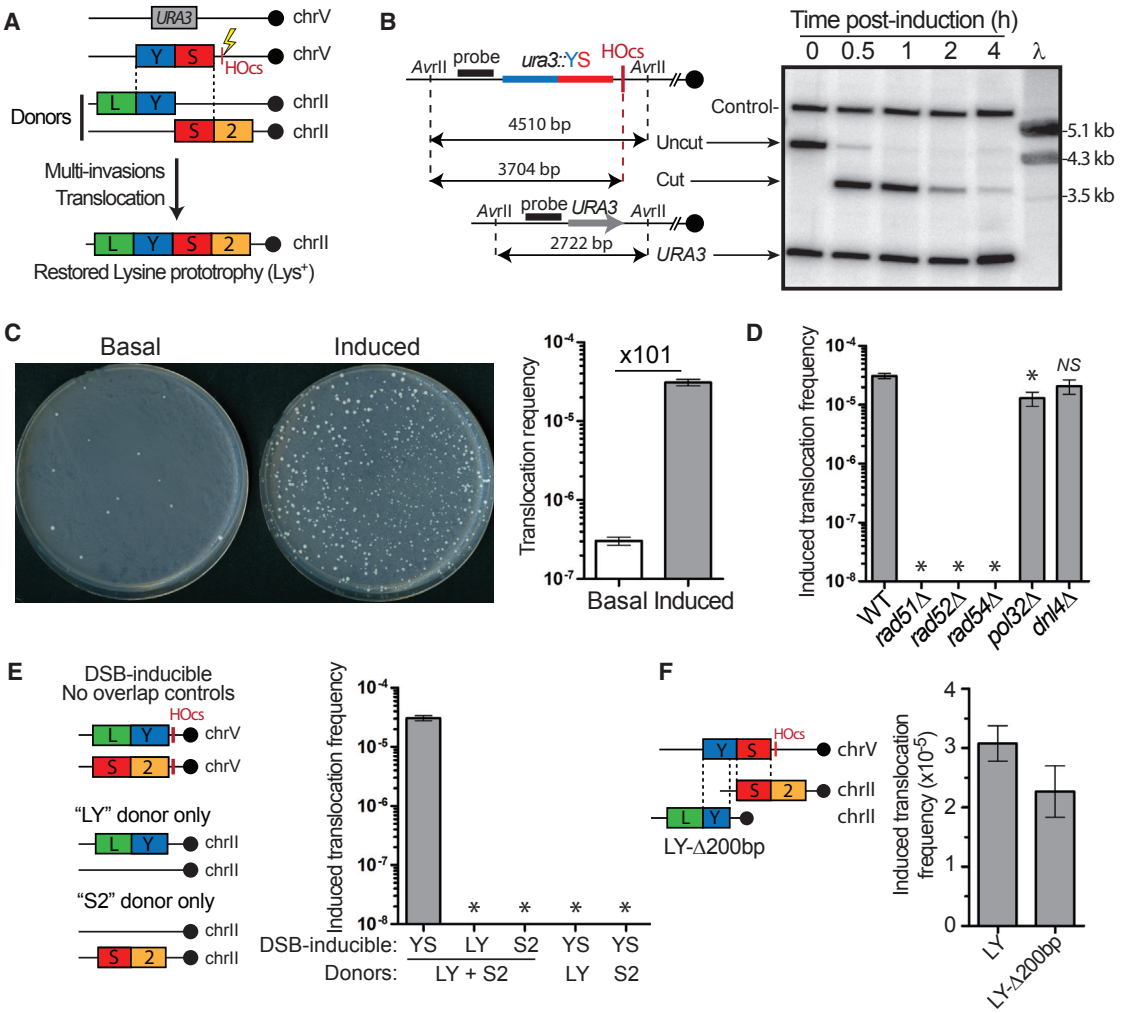

Figure 2. Requirements for Intact Chromosomal Regions Translocation Induced by a DSB on Another Molecule

(A) Reference tripartite recombination system in diploid yeast. The heterozygous DSB-inducible construct (YS-HOcs) replaces *URA3* on chrV. The LY and S2 donors represent the two halves of the *LYS2* gene and share no homology with one another. They are located in allelic configuration referred to as inter-chromosomal. Their blunt translocation restores a *LYS2* gene.

(B) Southern blot analysis of DSB kinetics upon HO induction. Predicted sizes (bp) for the uncut and cut locus as well as the other chrV homolog (*URA3*) upon *Avr*II digestion are shown on the left. Control, *RAD54* locus on chrVII; λ, length marker.

(C) DSB-induction causes a 101-fold increase in the translocation (Lys^+) frequency in wild-type. Representative SD-LYS plates with 5×10^7 cells plated are shown. Bars represent mean ± SEM. *$p < 0.05$.

(D) Induced translocation frequencies in wild-type, *rad51*Δ, *rad52*Δ, *rad54*Δ, *pol32*Δ, and *dnl4*Δ. No Lys^+ colonies are detected in the HR mutants at our detection limit ($\sim 10^{-8}$). Bars represent mean ± SEM. *$p < 0.05$.

(E) No Lys^+ colonies were observed with strains bearing DSB-inducible constructs devoid of homology overlap to the LY and S2 donors or strains lacking the LY or S2 donors. Bars represent mean ± SEM. *$p < 0.05$.

(F) Induced translocation frequency in the reference wild-type or a strain bearing an LY donor truncated for its last 200 bp (LY-Δ200 bp). Bars represent mean ± SEM. *$p < 0.05$.

See also Figure S2 and Table S3.

to loss of *MAT* heterozygosity (Figure S2C; STAR Methods), a positive regulator of HR in diploids (Heude and Fabre, 1993).

To corroborate this result, we triggered translocation in cells lacking the integrated break-inducible construct by transforming a linear dsDNA fragment bearing overlapping homology to the LY and S2 donors (Figure 3B). In this experiment, ≈90% of the transformed cells receive only one linearized molecule (STAR Methods). Transformation triggers normalized translocation frequencies comparable to those obtained with the chromosomally integrated construct (Figure 3B). Control transformations with an intact plasmid or lacking DNA did not yield any Lys^+ cells. Southern blot analysis of the translocants confirmed restoration of the *LYS2* gene in place of the donors (see below).

These two approaches demonstrate that a single broken molecule causes translocation of the homologous donors.

Translocation Requires Concomitant Invasions of the Two Donors

We next investigated whether translocation requires two concomitant invasions rather than successive individual invasions. We reasoned that if translocation requires the two invasions to happen in a short time frame, it should be strongly stimulated by (1) a greater homology search capacity conferred by increasing homology length (Forget and Kowalczykowski, 2012) and (2) the physical proximity of the donors, which will promote invasion of the second donor upon encounter with the first donor. These presuppositions were tested using a series of constructs depicted in Figure 3C.

First, translocation frequency increases more than linearly with the length of homology to both donors: a 5-fold decrease of both parts of the "YS" homology (in YS200-200) leads to a 750-fold drop in the translocation frequency. Conversely, lengthening homologies 2-fold (YS2000-2000) increases the translocation frequency 11-fold (Figure 3D). Hence, donor translocation is strongly stimulated by homology length, in stark contrast with the repair of a chromosomal DSB that requires only one invasion and is achieved with maximal efficiency with 200–300 bp of homology (Coïc et al., 2011; Inbar et al., 2000; Jinks-Robertson et al., 1993).

Second, physical tethering between the donors strongly stimulates translocation: the "intra-chromosomal" configuration yields translocation frequencies at least an order of magnitude higher than the inter-chromosomal configuration (Figure 3D). The extent of this increase is more pronounced for molecules harboring shorter homologies and hence more limited homology search capacity: 56-fold with YS200-200, 25-fold with YS1000-1000, and 18-fold with YS2000-2000 (Figure 3D). Astoundingly, the YS2000-2000 substrate with donors in the "intra" configuration reached a translocation frequency of almost 1%. This proximity effect is also significant when one of the donors is positioned ectopically on the same chromatid as the broken molecule (ectopic-*cis*) rather than on the homolog (ectopic-*trans*) (Figures 3C and 3E), although much less pronounced than upon tethering of the two donors in the intra configuration. Importantly, the ectopic and the intra-chromosomal donor configurations also rule out a requirement for flanking homologies around the LY and S2 donors for translocation formation.

Finally, we addressed possible differential requirements for the internal (Y) versus the DSB-proximal (S) homology region. Interestingly, a 5-fold length reduction of the DSB-proximal homology in YS1000-200 causes a 3.6-fold greater decrease of the translocation frequency than reducing the internal homology in YS200-1000 (Figure 3F). Reversing the orientation of these YS sequence variants indicates that this bias is position-specific, not sequence-specific (Figure S2D). Hence, favoring the formation of the internal over DSB-proximal invasion inhibits translocation. YS1000-200 is expected to perform the internal invasion of the LY donor first in 83% of the cases and only 17% of the case with YS200-1000 (Figure 3H) (Inbar and Kupiec, 1999). We surmised that cleavage of the 3′-proximal, homology-containing flap of the internal invasion product by Rad1-Rad10 (Fishman-Lobell and Haber, 1992) reduces the potential for MI (Figure 3H) and could account for the difference observed between YS1000-200 and YS200-1000. Consistently, deletion of *RAD1* stimulates translocation 6.6-fold with YS1000-200 (p value versus wild-type = 9.5×10^{-3}) to the same frequency as YS200-1000, which is induced only 1.5-fold (Figure 3G). Both constructs remain ≈12-fold lower than the reference YS construct, which is induced 2-fold compared to the wild-type strain. Hence, clipping of the Rad51-ssDNA by Rad1-Rad10 upon internal invasion protects against MI and ensuing rearrangements (Figure 3H).

These experiments support a mechanism by which one ssDNA molecule causes the translocation of two intact donors in a manner that requires their concomitant invasions. We termed this mechanism MIR.

Physical Evidence for MIs in Wild-Type Cells

In order to provide physical evidences for MI in cells, we developed "MI-Capture," a proximity ligation-based assay (de Wit and de Laat, 2012) that detects physical tethering of the LY and S2 donors (Figure 3I; STAR Methods). DNA-specific cross-linking of both heteroduplex DNAs constitutive of MI with psoralen leads to the covalent linkage of the LY and S2 donors, held together by the invading molecule. This tethering can be captured upon restriction digestion and ligation in dilute conditions of the unique sequences flanking the donors. The amount of the chimeric molecule produced is determined by quantitative PCR and reflects the amount of MIs in the cell population. This chimera is rare in the absence of DSB induction on chrV (Figure 3J) and likely corresponds to random inter-molecular ligation. Importantly, DSB induction resulted in donor tethering, as evident by chimeric ligation detection at 15-fold over background. This signal resulted from DNA strand invasions as it is reduced to background levels in a *rad51*Δ mutant. This DSB- and Rad51-dependent donor tethering demonstrates the existence of MI in cells.

The Mus81-Mms4, Yen1, and Slx1-Slx4 Nucleases Are Involved in MIR

Fusion of two presumably intact dsDNA donors upon invasion by a ssDNA molecule implies that the linearity of the donors is compromised during the translocation process. Joint DNA molecules are substrates for structure-selective endonucleases (SSEs), which recognize and cleave the structures formed at the boundaries of DNA strand exchange intermediates (Schwartz and Heyer, 2011). We addressed whether the conserved SSEs Mus81-Mms4, Yen1, and Slx1-Slx4 promote translocation. While single mutants do not significantly decrease translocation frequencies, any double mutant combination yields a significant 2-fold decrease (Figure 4A). This effect is independent of the varying degrees of viability in these strains (Figure S3A). The triple *mus81*Δ *yen1*Δ *slx1*Δ mutant shows a 6-fold decrease in translocation frequency (Figure 4A), not different from the elevated basal level observed in this strain (Figure S3B). Further deletion of *RAD1* does not affect either basal or induced translocation frequencies (Figures 4A and S3B). Furthermore, transient overexpression of a catalytic-deficient Mus81-D414A/D415A(dd)/Mms4 caused a 3-fold reduction of the induced translocation frequency (Figure S3A). This dominant-negative behavior suggests that the inactive heterodimer can occlude a substrate for the other nucleases. Thus, Mus81-Mms4, Slx1-Slx4, and Yen1 enable MIR in an overlapping fashion, likely by

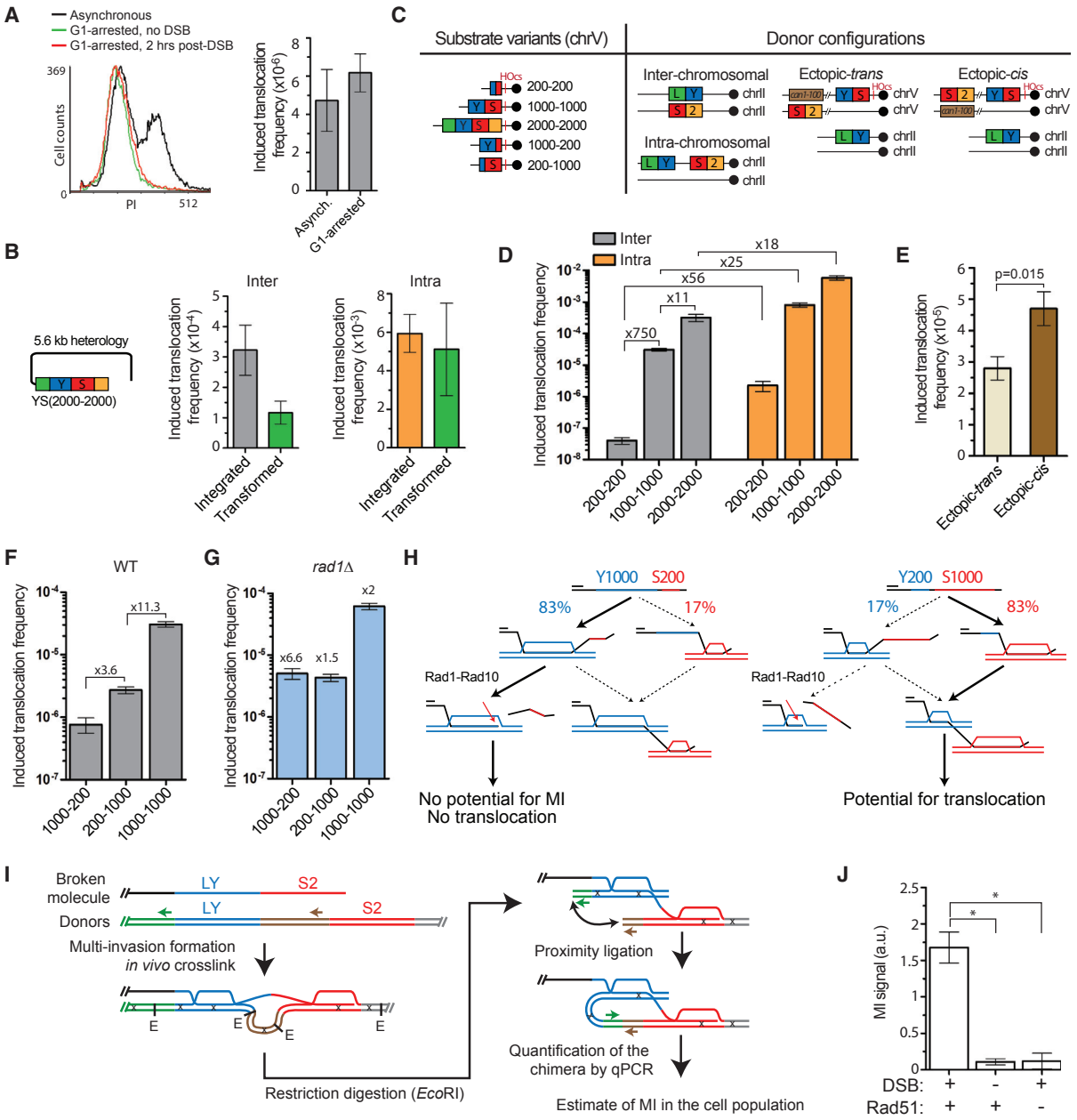

Figure 3. A Single ssDNA Molecule Concomitantly Invades Two Donors and Causes Their Translocation

(A) FACS profile and induced translocation frequency in asynchronous or G1-arrested cells. Bars represent mean ± SEM.

(B) Translocation frequency induced with either an integrated or a transformed YS2000-2000 construct in strains bearing the donors in the inter-chromosomal or intra-chromosomal configuration (Figure 3C).

(C) Scheme of substrate length variants and donor configurations. Bars represent mean ± SEM.

(D) Homology length and physical proximity of the donors stimulate translocation frequency in wild-type. Bars represent mean ± SEM.

(E) Induced translocation frequency in the ectopic-*trans* and ectopic-*cis* donor configurations. Bars represent mean ± SEM.

(F and G) Induced translocation frequency in wild-type (F) or *rad1*Δ (G) with asymmetric homology length variants. (G) Fold over wild-type is indicated. Bars represent mean ± SEM.

(H) Model for the Rad1-dependent differential effect of the DSB-proximal and -distal length of homology on MIR.

(I) Rationale of MI-Capture assay.

(J) The MI signal is DSB- and Rad51-dependent. Bars represent mean ± SEM of qPCR signal normalized over a control (*ARG4*) on chrVIII in wild-type either un-induced (n = 9) or 3 hr after DSB induction (n = 7), or in *rad51*Δ 3 hr after DSB induction (n = 3). *p < 0.05. Controls for HOcs cleavage and ligation efficiency are reported in Figures S2F and S2G.

See also Table S3.

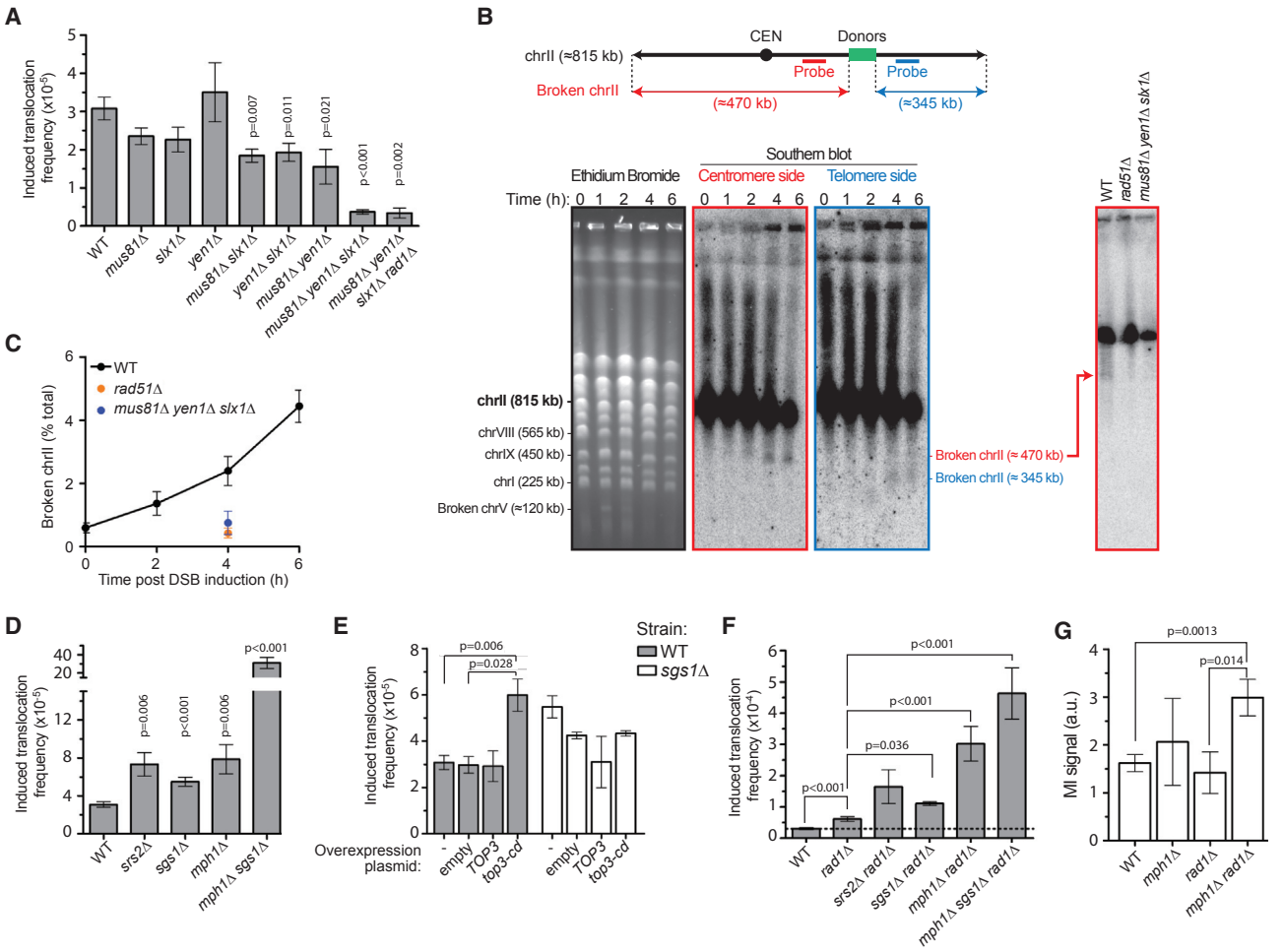

Figure 4. Genetic Controls of MIR

(A) Induced translocation frequencies in single or multiple mutants for *MUS81*, *SLX1*, and *YEN1*, as well as *mus81*Δ *slx1*Δ *yen1*Δ *rad1*Δ. Bars represent mean ± SEM.

(B) Physical evidence for chrII breakage at the donors following DSB induction on chrV (see Figure S3D) in a Rad51- and SSE-dependent fashion (right, 4 hr post-DSB induction).

(C) DSB quantification at donor site on chrII (n = 2). Bars represent mean ± SEM.

(D) Induced translocation frequency in the *srs2*Δ, *sgs1*Δ, *mph1*Δ, and *mph1*Δ *sgs1*Δ. Bars represent mean ± SEM.

(E) Induced translocation frequency in wild-type or *sgs1*Δ containing an empty overexpression plasmid or transiently overexpressing the WT or catalytic-deficient Top3. Bars represent mean ± SEM.

(F) Genetic interactions between *RAD1* and *SGS1*, *MPH1*, and *SRS2*. Bars represent mean ± SEM.

(G) MI levels 3 hr post-DSB induction in WT (n = 7), *mph1*Δ (n = 3), *rad1*Δ (n = 3), and *mph1*Δ *rad1*Δ (n = 9). Controls for DSB induction by HO and ligation efficiency are in Figure S3E and (F). Bars represent mean ± SEM.

See also Table S3.

cleaving DNA strand exchange intermediates constitutive of MI. Such redundancy for DNA joint molecule cleavage by these three SSEs has been reported previously (Muñoz-Galván et al., 2012; Pardo and Aguilera, 2012).

Physical Evidence for DSB Formation of the Donor Chromosome

To provide physical evidence for the recombination and SSE-dependent cleavage of the donors underlying MIR, we analyzed chrII integrity by pulse-field gel electrophoresis and Southern blot with probes located either on the centromere or telomere side of the donor sequence (Figure 4B). Following break induction on chrV (Figure S3D), we observed formation of two pieces of broken chrII centered on the location of the donors (Figures 4B and 4C). Importantly, this breakage of chrII is abolished both in the absence of Rad51 or SSEs (Figures 4B and 4C). These results demonstrate that the processing of DNA strand exchange intermediates by SSEs required for MIR leads to the formation of a DSB on the donor chromosome.

Srs2, Sgs1-Top3-Rmi1, Mph1, and Rad1-Rad10 Inhibit MIR

Several proteins have been implicated in joint molecules disruption during DSB repair by HR. The Srs2 helicase (Liu et al., 2017), the Mph1 helicase (Prakash et al., 2009), and the Sgs1-Top3-Rmi1 helicase-topoisomerase complex (Fasching et al., 2015) disrupt Rad51/Rad54-catalyzed D-loops in reconstituted reactions, consistent with their anti-recombination and/or anti-crossover function in yeast. We addressed whether these activities also inhibit MIR. Individual deletion of *SRS2*, *SGS1*, and *MPH1* all cause a significant 2- to 3-fold increase of the translocation frequency (Figure 4D). Transient overexpression of the dominant-negative, catalytic-deficient *top3-Y356F* allele (Oakley et al., 2002) phenocopied the *SGS1* deletion (Figure 4E). The translocation frequency did not increase further upon overexpression of *top3-Y356F* in a *sgs1*Δ strain (Figure 4E). This epistasis relationship is consistent with previous findings showing that the Top3 catalytic activity is required for the D-loop disruption activity of the STR complex (Fasching et al., 2015; Kaur et al., 2015; Tang et al., 2015). Furthermore, the *mph1*Δ *sgs1*Δ double mutant exhibits a 10-fold elevated translocation frequency compared to wild-type cells, more than the sum of the effects of the single mutants (Figure 4D). This synergy could result from the loss of their overlapping D-loop disruption activities (Prakash et al., 2009) or more complex relationships in the processing of the MI intermediate. Further genetic interactions with *SRS2* could not be investigated due to the HR-dependent synthetic growth defect of the double and triple mutants (Gangloff et al., 2000; Prakash et al., 2009).

We further investigated the interactions between the MIR suppression activity of Rad1-Rad10 and STR, Mph1, and Srs2. All the double and triple mutant combinations led to various degrees of increase in translocation frequency compared to any single mutant (Figure 4F). The activity of STR is additive to that of Rad1-Rad10, indicating independent functions in suppressing MIR, while deletion of *MPH1* and *RAD1* causes a synergistic, 10-fold increase of the translocation frequency. These genetic interactions indicate that Mph1, but not STR, removes a substrate for Rad1-Rad10 cleavage. These results suggest that Mph1 preferentially disrupts the internal invasions.

Finally, we determined the physical MI levels in cells defective for the Mph1 and Rad1-Rad10 activities. The *mph1*Δ *rad1*Δ strain exhibits a significant 2-fold increase in MIs (Figure 4G), whereas single mutants have no detectable effect. These results show that Mph1 and Rad1-Rad10 inhibit MIR by preventing accumulation of MI in cells. We conclude that multiple activities inhibit MIR by preventing MI formation and by disrupting the strand invasions constitutive of the MI intermediate.

Insights into the MIR Mechanism from the Physical Analysis of Translocants

To gain insights into the translocation mechanism and identify potential collateral rearrangements ensuing from donor cleavage by SSE, we analyzed Lys^+ translocants obtained in different donor configurations by Southern blot and qPCR for structural and copy-number variations, respectively. First, we analyzed basal (n = 11) and induced (n = 47) translocants in our reference strain bearing the donors in the allelic (inter-chromosomal) configuration. Because ≈10% of the Lys^+ colonies appeared small on the selection plates (Figure S4A), we analyzed them separately (10/47 induced, see below). The DSB-inducible YS-HOcs construct on chrV was retained in 8/11 cases in basal translocants. After DSB induction, 37/37 normal-sized and 9/10 small colonies had lost the YS-HOcs construct (Figures 5A and 6A) that was converted to *URA3* off the chrV homolog, as determined by qPCR (Figures 5B and S5A). Hence, a DSB at HOcs was formed in all the induced but likely in only a fraction of the basal translocants, which may have arisen by a different mechanism such as template-switch during the repair of an endogenously damaged donor (Hicks et al., 2010).

Southern blot analysis showed that *LYS2* was restored at its locus in all cases (Figure 5A), a result confirmed by Sanger sequencing of 18 translocants. The *LYS2* gene segregated either with the LY or the S2 donor (34/37). In the three remaining instances, the second chrII was lost (#22), bore a second *LYS2* gene (#25), or contained an additional chrII with both LY and S2 (#1) (Figures 5C and S5C). A similar pattern of donor retention is observed in translocants obtained by transformation (Figure S4B). Hence, in the inter-chromosomal configuration, the translocation mechanism mostly restores one *LYS2* gene per cell, which segregates with either the LY or the S2 donor present on the other homolog (Figure 5D). Analysis of 56 translocants induced with an inverted "YS" sequence near the DSB site confirmed this pattern (Figure S4C) and further revealed a preferential retention (≈2:1) of the DSB-proximal over the internal donor (Figure 5E). This segregation pattern indicates that the translocation can be carried by either donor and suggests the existence of two MIR pathways (see Discussion and Figures S7 and S8).

Additional Chromosomal Abnormalities Are Frequently Associated with MIR

Southern blot analysis identified additional structural variation (SV) involving chrII and chrV in 3/37 (8%) of normal and 4/10 (40%) of small Lys^+ colonies (Figures 5A and 6A). Further copy-number variation (CNV) determination by qPCR analysis revealed whole chrII and/or chrV aneuploidies in 1/37 of normal and 9/10 of small colonies (Figures S5B and S5C). Copy-number gains were typically low, from 1 to 2, but in some cases, copy numbers of 4 or 5 were observed (Figures S5B and S5C). In total, additional chromosomal alterations were found in 4/37 and 9/10 of the regular and small induced colonies, respectively (Figure 6B). This significantly higher prevalence of additional aberrations in small versus normal colonies likely accounts for their delayed appearance on –LYS plates. Given the proportion of small colonies (≈10%) and the frequency of rearrangements in both normal and small colonies, we estimate that in the inter-chromosomal configuration ≈15% of the MIR events are accompanied by additional SVs and/or CNV.

The Prevalence of Additional Chromosomal Abnormalities Depends on the Donor Configuration

In the inter-chromosomal configuration, the sequences flanking the LY and S2 donors are identical, presumably providing

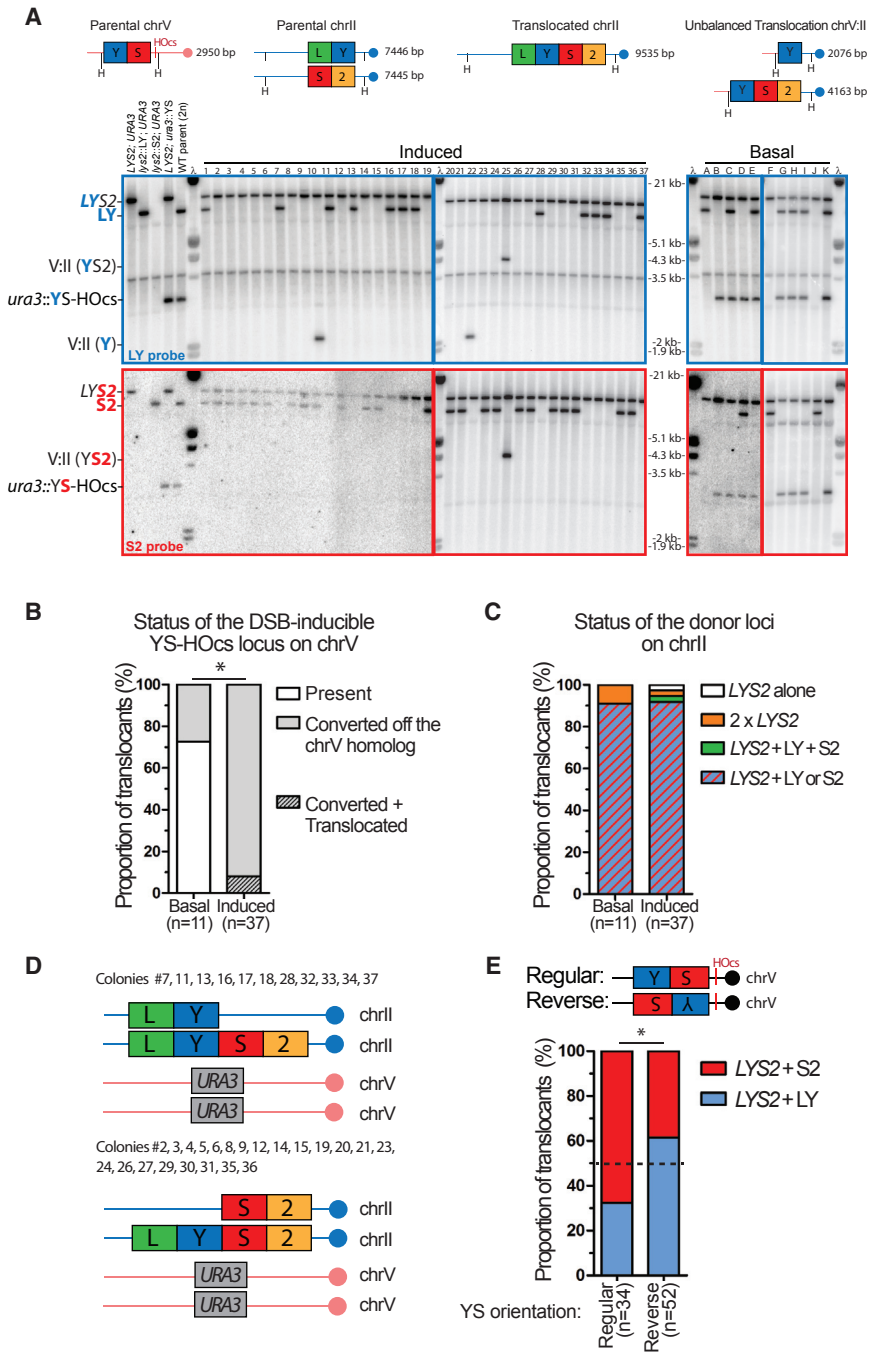

Figure 5. Physical Analysis of MIR Translocants

(A) Southern blot analysis of basal (n = 11) or induced Lys$^+$ cells (n = 37, normal colony size) obtained with the wild-type inter-chromosomal strain. The expected size of the parental and translocated molecules upon *Hind*III digestion is shown on the left. Blots were probed with either the LY (top, blue) or the S2 probe (bottom, red) and phage λ DNA (molecular ladder).

(B) Status of the DSB-inducible YS-HOcs construct in basal and induced cells. Translocated refers to chrV:II translocations depicted in (A). *$p < 0.05$, Fisher's exact test.

(C) Summary of the donor segregation pattern together with *LYS2*.

(D) Summary of the genetic content of normal-size translocants exhibiting no additional chromosomal abnormalities (33/37).

(E) The translocated *LYS2* gene segregates preferentially with the donor corresponding to the DSB-proximal homology. Southern blot analysis of translocants induced with a DSB-inducible construct bearing the YS sequence in reverse orientation is shown Figure S4C. *$p < 0.05$, Fisher's exact test.

opportunities for accurate repair of the two single-ended DSBs off an intact chromatid. To address whether the surrounding sequence context influences the capacity of MIR to generate additional rearrangements, we analyzed normal-size translocants obtained in the ectopic donor configurations (Figure 3C). Among 24 translocants obtained in the ectopic-*cis* (n = 12) and the ectopic-*trans* (n = 12) strains, all had restored *LYS2* in place of the S2 donor (Figures 6C and S5D), unlike the inter-chromosomal configuration in which *LYS2* replaces either the LY or the S2 donor (see Discussion). In addition, frequent additional SVs were observed in both the ectopic-*cis* and -*trans* contexts (7/12 each). Copy-number analysis by qPCR in the ectopic-*cis* translocants identified CNV of part or entire chrII and/or chrV in 7/12 cases, in addition to the terminal CNV associated with the non-reciprocal II:V(*LYS2*) translocation (Figures 6D and S5E). In total, 9/12 of ectopic-*cis* translocants exhibited an additional chromosomal abnormality (Figure S5F), significantly more than what is observed in the allelic inter-chromosomal configuration (Figure 6D).

In contrast to the inter-chromosomal, ectopic-*cis* and ectopic-*trans* configurations, additional rearrangements were not observed in the intra-chromosomal donor configuration (Figure S6A). MIR restored *LYS2* by deleting the short (1-kb) intervening sequence between the LY and S2 donors in all the translocants analyzed: basal, induced, or transformed (Figures S6A and S6B). We surmise that the short spacer DNA between the two single-ended DSBs is degraded before it can engage in additional rearrangements (Figure S6C).

These experiments show that MIR propagates single-ended DSBs on the donors, which undergo frequent additional rearrangements. The sequence context of the donors modulates the prevalence of these secondary rearrangements, either by providing opportunities for accurate DSB repair of the two single-ended DSBs by synthesis-dependent strand annealing

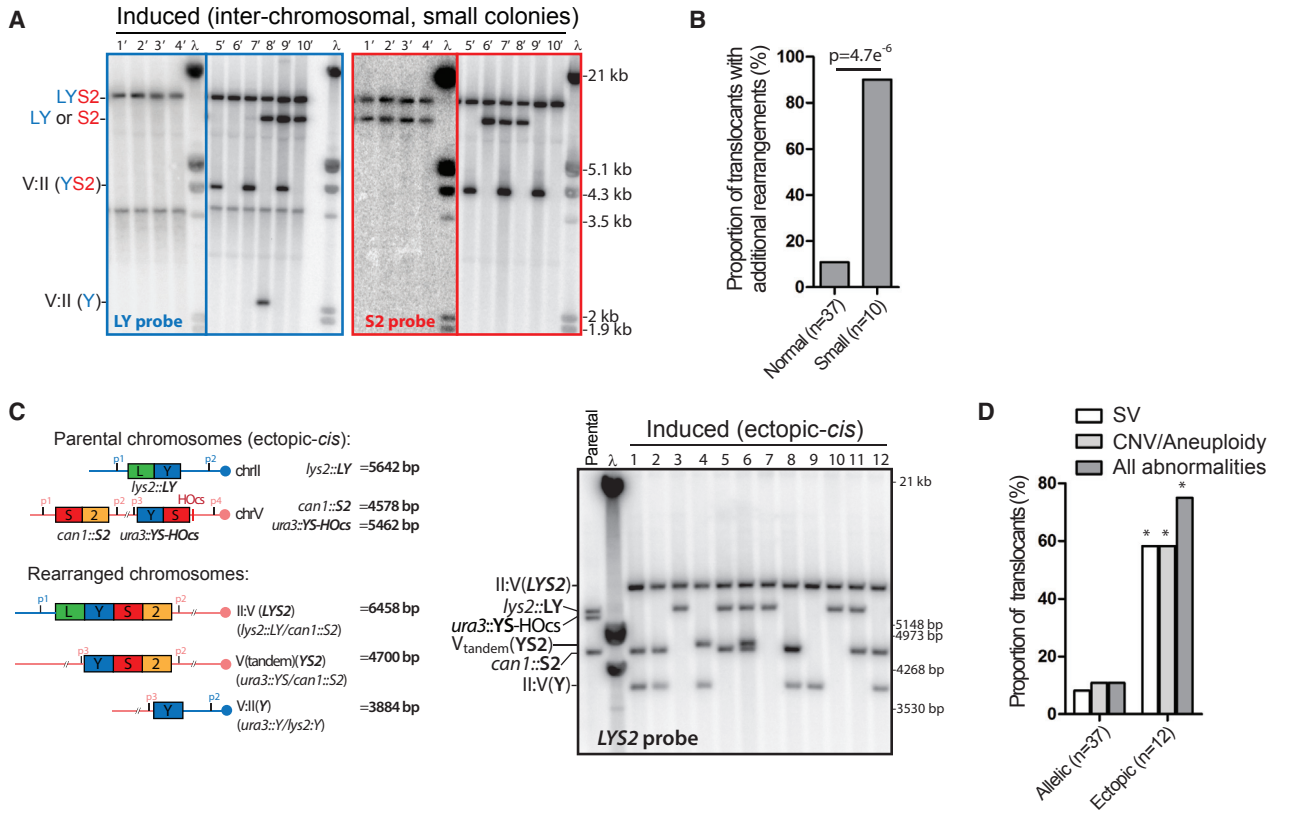

Figure 6. MIR Is Frequently Associated with Additional Chromosomal Abnormalities

(A) Southern blot analysis of induced Lys$^+$ cells (n = 10, small colony size) obtained with the reference inter-chromosomal strain. Other legends as in Figure 5A.

(B) Summary of additional chromosomal abnormalities in normal and small induced Lys$^+$ colonies.

(C) Southern blot analysis of induced translocants (n = 12, normal colonies) obtained with the ectopic-*cis* strain. The expected size of the parental and translocated molecules upon PstI digestion is shown on the left. Blots were hybridized with the *LYS2* probe and phage λ DNA (molecular ladder).

(D) Summary of the SV detected by Southern blot and the CNV/aneuploidies determined by qPCR in normal-size translocants obtained in the inter-chromosomal and the ectopic-*cis* donor configurations (Figures S5C and S5F). *p < 0.05, Fisher's exact test.

See also Figure S6.

(SDSA) (i.e., allelic inter-chromosomal) (Figure S7) or by causing their rapid elimination (i.e., intra-chromosomal) (Figure S6C).

DISCUSSION

Mechanisms of MIR

MIR is a genomic instability mechanism that causes translocation of two initially undamaged chromosomes upon breakage at a distinct locus. The danger of MI formation is inherent to the multiplexed homology search process during HR (Forget and Kowalczykowski, 2012; Wright and Heyer, 2014). Influences on MIR maturation by both the DNA substrate and proteins in DNA metabolism are outlined in Figure 7. Two specific mechanisms for MIR are proposed in Figure S7. They are consistent with the segregation profiles obtained in the allelic inter-chromosomal and the ectopic donor configurations, the preferential DSB-proximal (S2) donor retention observed in the inter-chromosomal configuration (Figure 5E), and the prevalence of additional rearrangements in the ectopic versus allelic donor configuration (Figure 6D). A model that accounts for the secondary rearrangements is proposed in Figure S8.

MIR and Other Tripartite Rearrangement Mechanisms

MIR is a tripartite recombination outcome with distinct origins from template-switch-prone DNA synthesis (Anand et al., 2014; Ruiz et al., 2009; Smith et al., 2007; Stafa et al., 2014) and a type of ends-out gene targeting technique called "bridge-induced translocation" (BIT) (Tosato et al., 2005). Despite similar sequence requirements, they differ in terms of the location and number of the initial breaks, the nature of the invasions, the extent of displacement DNA synthesis required, and the regulation by *trans*-acting factors.

BIT requires two DSBs, as it is induced by a linear dsDNA fragment with each extremity bearing homology to two different genomic locations. Priming of BIR from each extremity results in an additional chromosome with the intact dsDNA region inserted in the middle (Rossi et al., 2010). These dual DSBs are extremely unlikely in a physiological setting. In contrast, MIR is induced by a single DSB end, requires two types of invasions (DSB-proximal and -internal), and inserts the intervening ssDNA sequence between the two sites of invasions.

Template-switches are particularly frequent during the early stage of the Pol32-dependent DSB repair synthesis during BIR

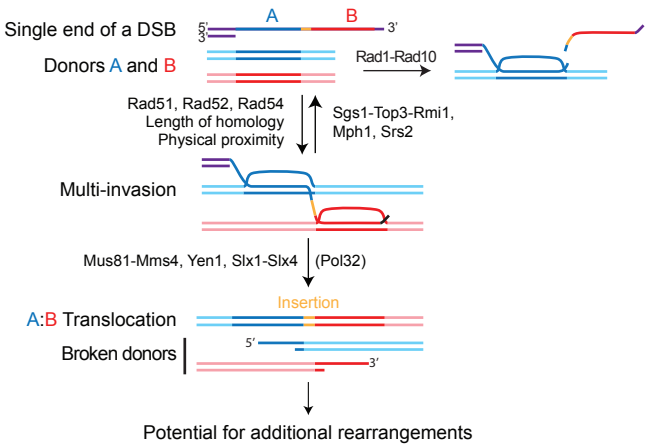

Figure 7. Model for MIR

One ssDNA molecule with homology to two donors A and B, without the need for homology to one another, can form a MI intermediate. Formation of MI is stimulated by homology length and physical proximity of the donors. Cleavage of the invading strand by Rad1-Rad10 upon internal invasion irreversibly prevents MI formation and protects against MIR. The Srs2 and Mph1 (human FANCM) helicases and the Sgs1-Top3-Rmi1 (human BLM-TOPOIIIα-RMI1-RMI2) helicase/topoisomerase complex disrupt MI and also inhibit MIR. Processing of MI by the overlapping activities of the Mus81-Mms4, Yen1, and Slx1-Slx4 SSE triggers MIR and transfers single-ended DSBs onto the donors. MIR occurs upon joining of the two opposite ends of the donors using the Rad51-ssDNA from the invading molecule as a synthesis template, which inserts sequence at the translocation junction. The two single-ended DSBs generated on the donors have potential to undergo secondary rearrangements. Detailed MIR mechanisms are proposed (see Figure S7).
See also Figure S8.

(Mayle et al., 2015). Initiation of template-switch requires a break on one of the external sequence (e.g., LY or S2 in our system) while MIR is initiated by a DSB onto the central sequence bearing the homology overlap. The two invasions of template-switch are successive, while MIR requires concomitant invasions. Extensive synthesis will then ensue until stabilization of the chromosome by capture of a telomeric sequence (Bosco and Haber, 1998). Hence, replication-based template-switch mechanisms are heavily reliant on Pol32 (Anand et al., 2014), unlike MIR, which shows little dependence on Pol32 (Figures 2D and S7). Moreover, template-switch is suppressed by the action of Mus81-Mms4 (Mayle et al., 2015) contrary to MIR that relies on it. Finally, the D-loop disruption activities of Mph1 and Srs2 promote template-switch (Ruiz et al., 2009; Stafa et al., 2014) but inhibit MIR.

Implications of MIR Features for the Analysis of Simple and Complex Chromosomal Rearrangements

Certain features of MIR have important implications for our understanding of simple and complex rearrangements observed in human pathologies.

- MIR rearranges two initially undamaged molecules upon invasion by a third broken one, questioning the prevailing assumption that sequences prone to rearrange are solely those "at risk" to break.
- MIR is initiated by the sequence on one side of the break. Consequently, single-ended DSBs such as those created upon fork collapse are sufficient to trigger MIR.
- MIR exploits homologies distant from the break site to generate translocation.
- MIR is a HR-based mechanism that can generate SV junctions devoid of homology usually thought to originate from end-joining (EJ) or microhomology/microsatellite-induced replication (MMIR)/microhomology-mediated break-induced replication (MMBIR) mechanisms.
- MIR causes templated sequence insertion at the SV junction, providing an alternative to template-switch mechanisms.
- MIR generates large-scale rearrangements without extensive DNA synthesis, as indicated by the minimal involvement of Pol32.
- From one end of a DSB, MIR can propagate up to two more single-ended DSBs, which can undergo additional rearrangements at high frequency. This break propagation capacity of MIR could participate of the cascade of breaks and rearrangements characteristic of chromothripsis (Korbel and Campbell, 2013).

The only sequence requirement for MIR is the presence of overlapping homology to two discontinuous genomic regions, preferentially in close physical proximity. In human, this represents a massive amount of potential sequences, as ~50% of the genome is comprised of repeats compatible in length (>200 bp) with MIR, such as remnants of mobile elements (0.1–7 kb) and segmental duplications (>5 kb). Rearrangements mediated by dispersed repeats have been implicated in human diseases (Carvalho and Lupski, 2016). For example, there are 492 reported de novo human pathologies associated with *Alu* element (~300 bp) recombination (Kim et al., 2016). The envisioned mechanism underlying these non-allelic homologous recombination (NAHR)-mediated rearrangements is the double-strand break repair (DSBR) model (Szostak et al., 1983), which entails the formation of a break within a repeat, two mismatched ectopic invasions, and resolution of the double Holliday junction (dHJ) intermediate into a crossover (CO). MIR more parsimoniously explains NAHR-mediated rearrangements than the DSBR model because it does not require the DSB to fall in the repeat but only in the span of resection. This expanded space for DSB formation could account for the perceived higher probability of DSB in *Alu* repeats (Shaw and Lupski, 2005) and the enrichment of binding sites for the meiotic DSB-eliciting enzyme PRDM9 not within, but at an average distance of 2 kb from the rearrangement-prone repeats (Dittwald et al., 2013). Consistently, in yeast, a break outside a Ty element is more prone to generate rearrangements than a DSB induced within (Hoang et al., 2010). Moreover, invasions on short homeologies typical of dispersed repeats strongly inhibit CO formation (Inbar et al., 2000), likely by precluding the dual invasions required for dHJ formation. MIR minimally requires one homeologous invasion, the second invasion most likely being allelic, on the sister chromatid or homologous chromosome. Finally, the DSBR model fails to explain tripartite recombination events, whose signature is accounted for by MIR. An example is given by an *Alu*-mediated deletion in the *SOX10* promoter responsible for

the Waardenburg Syndrome 4 in which two *Alu* elements located 56 kb apart were recombined by a third, more distant *Alu* element that inserted its sequence at the deletion junction (Bondurand et al., 2012). Similar tripartite repeat rearrangements have also been observed in yeast (Putnam et al., 2009; Thierry et al., 2015). Repeated elements also mediate complex chromosomal rearrangements (Carvalho and Lupski, 2016) and in certain cases chromothripsis (Nazaryan-Petersen et al., 2016).

Contexts Prone to MIR and Chromothripsis

Chromothripsis is a recently recognized genomic instability phenomenon associated with cancer and congenital disease (Korbel and Campbell, 2013; Stephens et al., 2011; Kloosterman and Cuppen, 2013). It is characterized by extensive and clustered genomic rearrangements affecting parts of one or few chromosomes thought to originate from a single catastrophic event rather than by incremental alterations over generations. The underlying mechanism(s) remain elusive: based on the translocation junction sequences that often lack homology and exhibit small insertions, and the oscillation of limited CNV states, EJ and replicative mechanisms have been proposed (Liu et al., 2011; Stephens et al., 2009, 2011). Recent experimental work involved EJ in chromothripsis induced by a lagging Y chromosome (Ly et al., 2017). Adding to the complexity of the etiology of chromothripsis, the enrichment for repeated sequences (Carvalho and Lupski, 2016; Nazaryan-Petersen et al., 2016) and for apolipoprotein B mRNA-editing enzyme (APOBEC)-induced mutational showers (kataegis) (Maciejowski et al., 2015; Nik-Zainal et al., 2012) at or near chromothriptic rearrangement junctions suggested the involvement of long ssDNA (Roberts et al., 2012) and HR repair. Further pointing at the involvement of HR, is the fact that tumors defective for p53, a known suppressor of HR (Mekeel et al., 1997), are enriched for chromothripsis (Rausch et al., 2012).

We have shown that long ssDNA, HR, and SSEs are essential for MIR, a mechanism that propagates additional single-ended DSBs while generating a translocation. A role of the nucleus is to restrict the access of cytoplasmic nucleases to DNA, as demonstrated for GEN1 (Chan and West, 2014). To date, chromothripsis has only been experimentally shown to result from defects in nuclear compartmentalization either in micronuclei causing extensive damage to replicating DNA (Ly et al., 2017; Zhang et al., 2015) or upon rupture of the nuclear envelope at the base of chromatin bridges (Maciejowski et al., 2015). In the latter study, exposure of the DNA of the bridge to the cytoplasmic TREX1 nuclease was shown to cause its resection and the snap back of massive amounts of ssDNA into the daughter nucleus where it triggered chromothripsis associated with kataegis. Because long ssDNAs are not substrate for EJ mechanisms, the chromothriptic rearrangements observed by Maciejowski et al. (2015) may have arisen from attempted HR repair. Another source of long ssDNA is BIR (Saini et al., 2013). A possible interplay between BIR and MIR is suggested by the unexpected inter-chromosomal rearrangements observed in addition to BIR products in yeast transformation experiments (Stafa et al., 2014). Consequently, contexts that generate long ssDNA for HR repair and/or compromise isolation of DNA from unscheduled endonucleolytic cleavage are prone to both MIR and chromothripsis. Our results further suggest that defects in proteins that disrupt DNA strand exchange intermediates should promote SV by MIR.

STAR★METHODS

Detailed methods are provided in the online version of this paper and include the following:

- KEY RESOURCES TABLE
- CONTACT FOR REAGENT AND RESOURCE SHARING
- EXPERIMENTAL MODEL AND SUBJECT DETAILS
  - Diploid *Saccharomyces cerevisiae* strains and constructions
  - Media and culture conditions
- METHOD DETAILS
  - Preparation of DNA substrates
  - Proteins
  - Reconstituted D-loop reactions
  - Southern Blots of D-loop reaction gels
  - Translocation assay in *S. cerevisiae*
  - Translocation assay upon transformation of a linearized plasmid
  - Translocation assay in G1-arrested cells and FACS analysis
  - Southern blot analysis of the translocants
  - Time course analysis of DSB formation on chrV by Southern blot
  - Analysis of DSB formation at the donors on chrII by pulse-field gel electrophoresis
  - ChrII and V copy number analysis by quantitative PCR
  - Multi-invasion-Capture assay
- QUANTIFICATION AND STATISTICAL ANALYSIS
- DATA AND SOFTWARE AVAILABILITY
  - Construct sequences

SUPPLEMENTAL INFORMATION

Supplemental Information includes eight figures, three tables, and one data file and can be found with this article online at http://dx.doi.org/10.1016/j.cell.2017.06.052.

AUTHOR CONTRIBUTIONS

A.P. and W.-D.H. conceived the project and wrote the manuscript, with input and editing from W.D.W. A.P. designed, performed, and analyzed the in vivo and some in vitro experiments. W.D.W. designed, performed, and analyzed most of the in vitro experiments.

ACKNOWLEDGMENTS

We thank members of the Heyer laboratory as well as Jim Haber and Martin Kupiec for helpful discussions. We are particularly thankful to Rodney Rothstein, Lorraine Symington, and Neil Hunter for their critical comments. We thank Abou Ibrahim-Biangoro and Noelle Cabral for help with strains construction. We are grateful to Adam Bailis, Lorraine Symington, Ian Hickson, Patrick Sung, Steve Kowalczykowski, Neil Hunter, and Marc Wold for strains and protein expression vectors. A.P. was supported by fellowships from the Fondation ARC pour la Recherche sur le Cancer, the EMBO (ALTF-238-2013), the Framework Project 7 of the European Union (Marie Curie International Outgoing Fellowship 628355) administered by the Institut Pasteur, France, and received financial support from the Philippe Foundation. This research was supported

by NIH grants GM58015 and CA92276 and award FBF 2015-32 from the France-Berkeley Fund to W.-D.H.

Received: January 10, 2017
Revised: May 2, 2017
Accepted: June 30, 2017
Published: August 3, 2017

REFERENCES

Anand, R.P., Tsaponina, O., Greenwell, P.W., Lee, C.S., Du, W., Petes, T.D., and Haber, J.E. (2014). Chromosome rearrangements via template switching between diverged repeated sequences. Genes Dev. *28*, 2394–2406.

Barlow, J.H., Lisby, M., and Rothstein, R. (2008). Differential regulation of the cellular response to DNA double-strand breaks in G1. Mol. Cell *30*, 73–85.

Bell, J.C., and Kowalczykowski, S.C. (2016). RecA: regulation and mechanism of a molecular search engine. Trends Biochem. Sci. *41*, 491–507.

Binz, S.K., Dickson, A.M., Haring, S.J., and Wold, M.S. (2006). Functional assays for replication protein A (RPA). Methods Enzymol. *409*, 11–38.

Bondurand, N., Fouquet, V., Baral, V., Lecerf, L., Loundon, N., Goossens, M., Duriez, B., Labrune, P., and Pingault, V. (2012). *Alu*-mediated deletion of SOX10 regulatory elements in Waardenburg syndrome type 4. Eur. J. Hum. Genet. *20*, 990–994.

Bosco, G., and Haber, J.E. (1998). Chromosome break-induced DNA replication leads to nonreciprocal translocations and telomere capture. Genetics *150*, 1037–1047.

Bugreev, D.V., and Mazin, A.V. (2004). Ca2+ activates human homologous recombination protein Rad51 by modulating its ATPase activity. Proc. Natl. Acad. Sci. USA *101*, 9988–9993.

Carvalho, C.M., and Lupski, J.R. (2016). Mechanisms underlying structural variant formation in genomic disorders. Nat. Rev. Genet. *17*, 224–238.

Chan, Y.W., and West, S.C. (2014). Spatial control of the GEN1 Holliday junction resolvase ensures genome stability. Nat. Commun. *5*, 4844.

Coïc, E., Martin, J., Ryu, T., Tay, S.Y., Kondev, J., and Haber, J.E. (2011). Dynamics of homology searching during gene conversion in *Saccharomyces cerevisiae* revealed by donor competition. Genetics *189*, 1225–1233.

de Wit, E., and de Laat, W. (2012). A decade of 3C technologies: insights into nuclear organization. Genes Dev. *26*, 11–24.

Dion, V., Kalck, V., Horigome, C., Towbin, B.D., and Gasser, S.M. (2012). Increased mobility of double-strand breaks requires Mec1, Rad9 and the homologous recombination machinery. Nat. Cell Biol. *14*, 502–509.

Dittwald, P., Gambin, T., Szafranski, P., Li, J., Amato, S., Divon, M.Y., Rodríguez Rojas, L.X., Elton, L.E., Scott, D.A., Schaaf, C.P., et al. (2013). NAHR-mediated copy-number variants in a clinical population: mechanistic insights into both genomic disorders and Mendelizing traits. Genome Res. *23*, 1395–1409.

Ehmsen, K.T., and Heyer, W.D. (2008). Saccharomyces cerevisiae Mus81-Mms4 is a catalytic, DNA structure-selective endonuclease. Nucleic Acids Res. *36*, 2182–2195.

Fabre, F., Chan, A., Heyer, W.D., and Gangloff, S. (2002). Alternate pathways involving Sgs1/Top3, Mus81/ Mms4, and Srs2 prevent formation of toxic recombination intermediates from single-stranded gaps created by DNA replication. Proc. Natl. Acad. Sci. USA *99*, 16887–16892.

Fasching, C.L., Cejka, P., Kowalczykowski, S.C., and Heyer, W.D. (2015). Top3-Rmi1 dissolve Rad51-mediated D loops by a topoisomerase-based mechanism. Mol. Cell *57*, 595–606.

Fishman-Lobell, J., and Haber, J.E. (1992). Removal of nonhomologous DNA ends in double-strand break recombination: the role of the yeast ultraviolet repair gene *RAD1*. Science *258*, 480–484.

Forget, A.L., and Kowalczykowski, S.C. (2012). Single-molecule imaging of DNA pairing by RecA reveals a three-dimensional homology search. Nature *482*, 423–427.

Gangloff, S., Soustelle, C., and Fabre, F. (2000). Homologous recombination is responsible for cell death in the absence of the Sgs1 and Srs2 helicases. Nat. Genet. *25*, 192–194.

Heude, M., and Fabre, F. (1993). a/alpha-control of DNA repair in the yeast *Saccharomyces cerevisiae*: genetic and physiological aspects. Genetics *133*, 489–498.

Heyer, W.D. (2015). Regulation of recombination and genomic maintenance. Cold Spring Harb. Perspect. Biol. *7*, a016501.

Hicks, W.M., Kim, M., and Haber, J.E. (2010). Increased mutagenesis and unique mutation signature associated with mitotic gene conversion. Science *329*, 82–85.

Hoang, M.L., Tan, F.J., Lai, D.C., Celniker, S.E., Hoskins, R.A., Dunham, M.J., Zheng, Y., and Koshland, D. (2010). Competitive repair by naturally dispersed repetitive DNA during non-allelic homologous recombination. PLoS Genet. *6*, e1001228.

Inbar, O., and Kupiec, M. (1999). Homology search and choice of homologous partner during mitotic recombination. Mol. Cell. Biol. *19*, 4134–4142.

Inbar, O., Liefshitz, B., Bitan, G., and Kupiec, M. (2000). The relationship between homology length and crossing over during the repair of a broken chromosome. J. Biol. Chem. *275*, 30833–30838.

Jinks-Robertson, S., Michelitch, M., and Ramcharan, S. (1993). Substrate length requirements for efficient mitotic recombination in *Saccharomyces cerevisiae*. Mol. Cell. Biol. *13*, 3937–3950.

Kaur, H., De Muyt, A., and Lichten, M. (2015). Top3-Rmi1 DNA single-strand decatenase is integral to the formation and resolution of meiotic recombination intermediates. Mol. Cell *57*, 583–594.

Kim, S., Cho, C.S., Han, K., and Lee, J. (2016). Structural variation of *Alu* element and human disease. Genomics Inform. *14*, 70–77.

Kloosterman, W.P., and Cuppen, E. (2013). Chromothripsis in congenital disorders and cancer: similarities and differences. Curr. Opin. Cell Biol. *25*, 341–348.

Kolodner, R.D., Putnam, C.D., and Myung, K. (2002). Maintenance of genome stability in *Saccharomyces cerevisiae*. Science *297*, 552–557.

Korbel, J.O., and Campbell, P.J. (2013). Criteria for inference of chromothripsis in cancer genomes. Cell *152*, 1226–1236.

Liu, P., Erez, A., Nagamani, S.C., Dhar, S.U., Kołodziejska, K.E., Dharmadhikari, A.V., Cooper, M.L., Wiszniewska, J., Zhang, F., Withers, M.A., et al. (2011). Chromosome catastrophes involve replication mechanisms generating complex genomic rearrangements. Cell *146*, 889–903.

Liu, J., Ede, C., Wright, W.D., Gore, S.K., Jenkins, S.S., Freudenthal, B.D., Todd Washington, M., Veaute, X., and Heyer, W.D. (2017). Srs2 promotes synthesis-dependent strand annealing by disrupting DNA polymerase δ-extending D-loops. eLife *6*, e22195.

Ly, P., Teitz, L.S., Kim, D.H., Shoshani, O., Skaletsky, H., Fachinetti, D., Page, D.C., and Cleveland, D.W. (2017). Selective Y centromere inactivation triggers chromosome shattering in micronuclei and repair by non-homologous end joining. Nat. Cell Biol. *19*, 68–75.

Lydeard, J.R., Jain, S., Yamaguchi, M., and Haber, J.E. (2007). Break-induced replication and telomerase-independent telomere maintenance require Pol32. Nature *448*, 820–823.

Maciejowski, J., Li, Y., Bosco, N., Campbell, P.J., and de Lange, T. (2015). Chromothripsis and kataegis induced by telomere crisis. Cell *163*, 1641–1654.

Mayle, R., Campbell, I.M., Beck, C.R., Yu, Y., Wilson, M., Shaw, C.A., Bjergbaek, L., Lupski, J.R., and Ira, G. (2015). DNA REPAIR. Mus81 and converging forks limit the mutagenicity of replication fork breakage. Science *349*, 742–747.

Mazón, G., and Symington, L.S. (2013). Mph1 and Mus81-Mms4 prevent aberrant processing of mitotic recombination intermediates. Mol. Cell *52*, 63–74.

Mekeel, K.L., Tang, W., Kachnic, L.A., Luo, C.M., DeFrank, J.S., and Powell, S.N. (1997). Inactivation of p53 results in high rates of homologous recombination. Oncogene *14*, 1847–1857.

Miné-Hattab, J., and Rothstein, R. (2012). Increased chromosome mobility facilitates homology search during recombination. Nat. Cell Biol. *14*, 510–517.

Muñoz-Galván, S., Tous, C., Blanco, M.G., Schwartz, E.K., Ehmsen, K.T., West, S.C., Heyer, W.D., and Aguilera, A. (2012). Distinct roles of Mus81, Yen1, Slx1-Slx4, and Rad1 nucleases in the repair of replication-born double-strand breaks by sister chromatid exchange. Mol. Cell. Biol. *32*, 1592–1603.

Nazaryan-Petersen, L., Bertelsen, B., Bak, M., Jønson, L., Tommerup, N., Hancks, D.C., and Tümer, Z. (2016). Germline chromothripsis driven by L1-mediated retrotransposition and *Alu/Alu* homologous recombination. Hum. Mutat. *37*, 385–395.

Nik-Zainal, S., Alexandrov, L.B., Wedge, D.C., Van Loo, P., Greenman, C.D., Raine, K., Jones, D., Hinton, J., Marshall, J., Stebbings, L.A., et al.; Breast Cancer Working Group of the International Cancer Genome Consortium (2012). Mutational processes molding the genomes of 21 breast cancers. Cell *149*, 979–993.

Nimonkar, A.V., Dombrowski, C.C., Siino, J.S., Stasiak, A.Z., Stasiak, A., and Kowalczykowski, S.C. (2012). *Saccharomyces cerevisiae* Dmc1 and Rad51 proteins preferentially function with Tid1 and Rad54 proteins, respectively, to promote DNA strand invasion during genetic recombination. J. Biol. Chem. *287*, 28727–28737.

Oakley, T.J., Goodwin, A., Chakraverty, R.K., and Hickson, I.D. (2002). Inactivation of homologous recombination suppresses defects in topoisomerase III-deficient mutants. DNA Repair (Amst.) *1*, 463–482.

Pardo, B., and Aguilera, A. (2012). Complex chromosomal rearrangements mediated by break-induced replication involve structure-selective endonucleases. PLoS Genet. *8*, e1002979.

Prakash, R., Satory, D., Dray, E., Papusha, A., Scheller, J., Kramer, W., Krejci, L., Klein, H., Haber, J.E., Sung, P., and Ira, G. (2009). Yeast Mph1 helicase dissociates Rad51-made D-loops: implications for crossover control in mitotic recombination. Genes Dev. *23*, 67–79.

Putnam, C.D., Hayes, T.K., and Kolodner, R.D. (2009). Specific pathways prevent duplication-mediated genome rearrangements. Nature *460*, 984–989.

Rausch, T., Jones, D.T., Zapatka, M., Stütz, A.M., Zichner, T., Weischenfeldt, J., Jäger, N., Remke, M., Shih, D., Northcott, P.A., et al. (2012). Genome sequencing of pediatric medulloblastoma links catastrophic DNA rearrangements with TP53 mutations. Cell *148*, 59–71.

Roberts, S.A., Sterling, J., Thompson, C., Harris, S., Mav, D., Shah, R., Klimczak, L.J., Kryukov, G.V., Malc, E., Mieczkowski, P.A., et al. (2012). Clustered mutations in yeast and in human cancers can arise from damaged long single-strand DNA regions. Mol. Cell *46*, 424–435.

Rossi, B., Noel, P., and Bruschi, C.V. (2010). Different aneuploidies arise from the same bridge-induced chromosomal translocation event in *Saccharomyces cerevisiae*. Genetics *186*, 775–790.

Ruiz, J.F., Gómez-González, B., and Aguilera, A. (2009). Chromosomal translocations caused by either pol32-dependent or pol32-independent triparental break-induced replication. Mol. Cell. Biol. *29*, 5441–5454.

Saini, N., Ramakrishnan, S., Elango, R., Ayyar, S., Zhang, Y., Deem, A., Ira, G., Haber, J.E., Lobachev, K.S., and Malkova, A. (2013). Migrating bubble during break-induced replication drives conservative DNA synthesis. Nature *502*, 389–392.

Schwartz, E.K., and Heyer, W.D. (2011). Processing of joint molecule intermediates by structure-selective endonucleases during homologous recombination in eukaryotes. Chromosoma *120*, 109–127.

Shaw, C.J., and Lupski, J.R. (2005). Non-recurrent 17p11.2 deletions are generated by homologous and non-homologous mechanisms. Hum. Genet. *116*, 1–7.

Smith, C.E., Llorente, B., and Symington, L.S. (2007). Template switching during break-induced replication. Nature *447*, 102–105.

Sneeden, J.L., Grossi, S.M., Tappin, I., Hurwitz, J., and Heyer, W.D. (2013). Reconstitution of recombination-associated DNA synthesis with human proteins. Nucleic Acids Res. *41*, 4913–4925.

Spies, J., Waizenegger, A., Barton, O., Sürder, M., Wright, W.D., Heyer, W.D., and Löbrich, M. (2016). Nek1 regulates Rad54 to orchestrate homologous recombination and replication fork stability. Mol. Cell *62*, 903–917.

Stafa, A., Donnianni, R.A., Timashev, L.A., Lam, A.F., and Symington, L.S. (2014). Template switching during break-induced replication is promoted by the Mph1 helicase in *Saccharomyces cerevisiae*. Genetics *196*, 1017–1028.

Stephens, P.J., McBride, D.J., Lin, M.L., Varela, I., Pleasance, E.D., Simpson, J.T., Stebbings, L.A., Leroy, C., Edkins, S., Mudie, L.J., et al. (2009). Complex landscapes of somatic rearrangement in human breast cancer genomes. Nature *462*, 1005–1010.

Stephens, P.J., Greenman, C.D., Fu, B., Yang, F., Bignell, G.R., Mudie, L.J., Pleasance, E.D., Lau, K.W., Beare, D., Stebbings, L.A., et al. (2011). Massive genomic rearrangement acquired in a single catastrophic event during cancer development. Cell *144*, 27–40.

Symington, L.S. (2016). Mechanism and regulation of DNA end resection in eukaryotes. Crit. Rev. Biochem. Mol. Biol. *51*, 195–212.

Szostak, J.W., Orr-Weaver, T.L., Rothstein, R.J., and Stahl, F.W. (1983). The double-strand-break repair model for recombination. Cell *33*, 25–35.

Tang, S., Wu, M.K.Y., Zhang, R., and Hunter, N. (2015). Pervasive and essential roles of the Top3-Rmi1 decatenase orchestrate recombination and facilitate chromosome segregation in meiosis. Mol. Cell *57*, 607–621.

Thierry, A., Khanna, V., Créno, S., Lafontaine, I., Ma, L., Bouchier, C., and Dujon, B. (2015). Macrotene chromosomes provide insights to a new mechanism of high-order gene amplification in eukaryotes. Nat. Commun. *6*, 6154.

Tosato, V., Waghmare, S.K., and Bruschi, C.V. (2005). Non-reciprocal chromosomal bridge-induced translocation (BIT) by targeted DNA integration in yeast. Chromosoma *114*, 15–27.

Van Komen, S., Macris, M., Sehorn, M.G., and Sung, P. (2006). Purification and assays of *Saccharomyces cerevisiae* homologous recombination proteins. Methods Enzymol. *408*, 445–463.

Wilson, T.E., Grawunder, U., and Lieber, M.R. (1997). Yeast DNA ligase IV mediates non-homologous DNA end joining. Nature *388*, 495–498.

Wright, W.D., and Heyer, W.D. (2014). Rad54 functions as a heteroduplex DNA pump modulated by its DNA substrates and Rad51 during D loop formation. Mol. Cell *53*, 420–432.

Zhang, C.Z., Spektor, A., Cornils, H., Francis, J.M., Jackson, E.K., Liu, S., Meyerson, M., and Pellman, D. (2015). Chromothripsis from DNA damage in micronuclei. Nature *522*, 179–184.

STAR★METHODS

KEY RESOURCES TABLE

REAGENT or RESOURCE	SOURCE	IDENTIFIER
Chemicals, Peptides, and Recombinant Proteins		
Trioxsalen (for MI-Capture assay)	Sigma-Aldrich	Cat#T6137
NuSieve GTG agarose (For PFGE analysis)	Lonza	Cat#50080
Seakem Gold Agarose (For PFGE analysis)	Lonza	Cat#50150
Alpha-factor mating pheromone	Sigma-Aldrich	Cat#T6901
Critical Commercial Assays		
Roche LightCycler 480 SYBR Green I Master (for CNV determination in translocants and for MI-Capture assay)	Roche	Cat#04707516001
DECAprime II labeling kit	Ambion	Cat#AM1455
Experimental Models: Organisms/Strains		
Saccharomyces cerevisiae; Individual genotypes see Table S1	N/A	N/A
Oligonucleotides		
Quantitative PCR primers, see Table S2	N/A	N/A
Recombinant DNA		
Annotated sequences of yeast constructs and plasmids available in Data S1.	N/A	N/A
Software and Algorithms		
Roche LightCycler 480 Software version 1.5.0	Roche	N/A
R x64 version 3.2.0	CRAN project	N/A
Cyflogic version 1.2.1.	Cyflogic	N/A

CONTACT FOR REAGENT AND RESOURCE SHARING

Further information and requests for resources and reagents should be directed to and will be fulfilled by the Lead Contact, Wolf-Dietrich Heyer (wdheyer@ucdavis.edu).

EXPERIMENTAL MODEL AND SUBJECT DETAILS

Diploid *Saccharomyces cerevisiae* strains and constructions

The genotype of the diploid *Saccharomyces cerevisiae* strains (W303 *RAD5*$^{+}$ background) used in this study are listed Table S1. We established this system in diploid cells, which represents its physiological ploidy, to provide a better model for other diploid organisms such as human. Moreover, diploidy buffers for rearrangements that may cause loss of essential genes and allow to capture more events than haploids. Strains contain a heterozygous copy of the *HO* endonuclease gene under the control of the *GAL1/10* promoter at the *TRP1* locus on chromosome (chr) IV. The HO cut-site at the mating-type loci (*MAT*) on chrIII is inactivated by point mutations to prevent HO cleavage (*MAT*a-inc/*MAT*α-inc). The heterozygous DSB-inducible construct upon HO expression replaces *URA3* on one Ch. V (−16 to +855 from the start codon) and the LY and S2 donors replace the original *LYS2* ORF on chrII in the reference (allelic inter-chromosomal) strain. The *URA3* locus on chrV and of the *LYS2* locus on chrII have been chosen because of their interstitial, untethered location that represent a maximally demanding homology search situation and which have been extensively used by others to study ectopic HR repair (Inbar and Kupiec, 1999; Miné-Hattab and Rothstein, 2012). The DSB-inducible construct contains the 117 bp HO cut-site (Fishman-Lobell and Haber, 1992) and a multiple cloning site in which various fragments of the 4179 bp-long *LYS2* gene have been cloned between the *Sac*I and *Sal*I sites. In the intra-chromosomal construct, a 1,018 bp insert containing the *HIS3* gene is inserted in the *LYS2* gene at its endogenous locus so as to split the gene exactly in the LY and S2 parts used in the inter-chromosomal construct. In the intra-chromosomal construct used for the MI-Capture assay, an unique 199 bp fragment of the PhiX genome containing an *Eco*RI site was added immediately 5′ of the S2 donor. In the ectopic-*cis* and -*trans* strains, the S2 donor and its 70 bp long terminator (together with *HIS3* for selection purposes) were inserted at the constitutively mutated *can1-100* locus, which caused a deletion of the beginning of the gene (−342 to +439 bp from the start codon). S2 was oriented so as to avoid generating a

dicentric II:V chromosome upon translocation with the LY donor left on chrII. Annotated sequences for each construct are available as .ape files in Data S1.

Constructs for the overexpression of the wild-type and catalytic-deficient (Top3-Y356F) versions of Top3 under the control of the *GAL1/10* promoter on a 2μ pYES2 plasmid were kindly provided by Dr. Hickson (Oakley et al., 2002). Vectors for overexpression of *MMS4* (pWDH591), *MUS81* (pWDH592), *MUS81-MMS4* (pWDH595), and catalytic-deficient *mus81-D414A/D415A(dd)-MMS4* (pWDH596) have been described previously (Ehmsen and Heyer, 2008). Mus81 and Mms4 bear N-terminal tags, His10-Flag and GST respectively, that do not affect their in vivo functions (Ehmsen and Heyer, 2008). *rad52::TRP1*, *dnl4::LEU2* and *rad1::LEU2* mutants were kindly provided by Dr. Bailis, and *pol32::kanMX* and *sgs1::HIS3* by Dr. Symington. *rad51::natMX* deletion was performed by a single-step replacement with short flanking homologies upon *natMX* amplification from pAG25 using primers 5′-AAGAGCA GACGTAGTTATTTGTTAAAGGCCTACTAATTTGTTATCGTCATcgccagatctgtttagcttgc and 5′-AGAATTGAAAGTAAACCTGTGTAAA TAAATAGAGACAAGAGACCAAATACctggatggcggcgttagtat. Genomic DNA for the amplification of the deletion cassettes of *yen1::hphMX*, *slx1::natMX*, and *mph1::kanMX* have been kindly provided by Dr. Hunter, *mus81::kanMX* by Allan Chan.

Media and culture conditions

Synthetic dropout and rich YPD (1% yeast extract, 2% peptone, 2% dextrose) solid and liquid media have been prepared according to standard protocols. Liquid YEP-lactate (1% yeast extract, 2% peptone, 2% Lactate) and Lactate-URA (0.17% Yeast Nitrogen Base, 0.5% Ammonium Sulfate, 0.2% amino acids dropout, 2% Lactate) were made using 60% Sodium DL-lactate syrup. All the cultures were performed at 30°C.

METHOD DETAILS

Preparation of DNA substrates

Procedure for dsDNA donors and long ssDNA substrates preparation have been previously described in detail (Wright and Heyer, 2014). The ds98-*1201* substrate is as described (Wright and Heyer, 2014) and the substrates bearing ~400 nt-long A and B homologies have been created using a similar strategy. Briefly, 402-nt fragments from the φX174 (A part) and *S. cerevisiae* (B part) genomes have been amplified with primers to introduce *Hind*III/*Nco*I (*lower case is genome homologies* A: 5′-CGTAAAGCTTCCATGggcc tactgcgactaaaga; B: 5′-CGTAAAGCTTCCATGgtctcaagttcaagttcaagaaca) and *Xba*I/PstI (A: 5′-CGTATCTAGACTGCAgaagtcatgatt gaatcg ; B: 5′-CGTATCTAGACTGCAGcgtttagcaacttatctg) restriction sites, as in (Wright and Heyer, 2014). Both A and B amplifications were digested with *Hind*III and *Xba*I and added to a ligation reaction with *Hind*III-linearized modified pBlueScript vector (pBSbase). The ligation was transformed into XLI-Blue *E. coli* and transformants were screened to obtain the desired chimeric A/B sequence plasmid (pWDH1180). From this plasmid, the circular ssDNA produced from ssDNA-rescue from *E. coli* can be cleaved with *Nco*I after the annealing of 5′ and 3′ cleavage oligonucleotides (5′-GACCATGGAAGCTTGATAT and 5′-GATAAGCTTC CATGGTCT, respectively), to produce a 824 nt ssDNA fragment ss4-*B401*-ss17-*A402* (italics denote homology to plasmid donor A or B). Alternatively, 5′ SmaI or 3′ *Eco*72I cleavage oligonucleotides can be annealed and digested by those enzymes to yield 1,040 nt ss141-*B402*-ss17-*A402*-ss78. The invariant other details of the cleavage reaction and DNA fragment purification are as described in (Wright and Heyer, 2014). The annotated sequence of the substrates are provided in Data S1.

Supercoiled circular dsDNA donors A (φX174-derived) and B (*RAD51* gene sequence) were constructed and purified by triton lysis and on CsCl gradients as described in (Wright and Heyer, 2014). A* is the 5,386 bp φX174 replicative form I DNA (New England Biolabs). Linear dsDNA donor A (401 bp) with 100 bp 5′ and 200 bp 3′ flanking heterologies was amplified from the φX174 genome with primers 5′-GCCGAAGAAGCTGGAGTAAC and 5′-GGTTATTGTCTCATGAGCGG, linear dsDNA donor A (1201 bp) with ~100 bp of heterologies on each side was amplified from plasmid A with primers 5′- GGTTATTGTCTCATGAGCGG and 5′- GTCGATTTTTGT GATGCTCGTC, and linear dsDNA donor B (piece of *RAD51*) with 200 bp 5′ and 400 bp 3′ heterologies was amplified from the *S. cerevisiae* genome with primers 5′- CGTCATTTCCGCTATTTCTGTCC and 5′- GGCAGCAGCATCCAGAAG. Both linear donors were purified on column following manufacturer instructions (Bioneer), ethanol precipitated and resuspended in 10 mM Tris pH 8.0 and 1 mM EDTA pH 8.0.

Proteins

S. cerevisiae Rad51 (Van Komen et al., 2006), Rad54 (Nimonkar et al., 2012), and RPA (Binz et al., 2006) were purified as described. Human RAD51 and RPA were purified as described (Sneeden et al., 2013). Human RAD54 was purified as described (Spies et al., 2016).

Reconstituted D-loop reactions

DNA substrates were end-labeled with T4 PNK (NEB) at 10X working concentration and were used in D-loop reactions directly after PNK heat inactivation as described (Wright and Heyer, 2014). The conditions of the D-loop reactions and the processing of samples were identical to (Wright and Heyer, 2014), except for DNA concentrations. Since the larger A* plasmid (5.4 kb) harbors more supercoils than A (3 kb), A* is favored in the competitive situation and so to produce roughly equal levels of primary invasions, less A* donor was used (5.4 μM bp) relative to A (21 μM bp). Briefly, in a reaction buffer containing 35 mM Tris-acetate pH 7.5, 100 mM NaCl, 7 mM magnesium-acetate, 2 mM ATP, 1 mM DTT, 0.25 mg/ml BSA, 20 mM phosphocreatine and 100 μg/ml phosphocreatine kinase,

Rad51 is added with ssDNA substrate for 10 min at 30°C, followed by RPA for 10 min after which Rad54 is added with donor dsDNA and incubation is continued for 20 min. Rad51 is present at 1 monomer to 3 nt or bp on the invading DNA, RPA at 1 heterotrimer to 25 nt ssDNA, and Rad54 at 12 monomers per molecule of donor plasmid. The D-loop reaction with human proteins was performed as above with the exception of the reaction buffer, which contained 30 mM Tris-HCl pH 7.5, 2 mM $CaCl_2$, 2 mM $MgCl_2$, 50 mM KCl, 1 mM ATP, 0.25 mg/ml BSA, 1 mM TCEP, 10 mM di-Tris phosphocreatine, and 0.1 mg/ml phosphocreatine kinase.

Southern Blots of D-loop reaction gels

D-loop reactions with unlabeled ssDNA or reactions stored at 4°C until radioactivity decayed to background were separated on 1% agarose gels, transferred onto a Hybond-XL membrane (GE healthcare) according to manufacturer instructions, and hybridized with radio-labeled A or A*-specific probes. The "A" specific probe template was a 500 bp fragment of the β-galactosidase gene (obtained by PCR with primers 5′ CAAGGCGAGTTACATGATC and 5′ GAGTATTCAACATTTCCGT) while the "A*" specific probe template was a 479 bp fragment of φX174 genome (obtained by PCR with primers 5′ TTGAGTGTGAGGTTATAAC and 5′ GAAGGACGTCAAT AGTCAC).

Translocation assay in *S. cerevisiae*

An overnight liquid YPD pre-culture was used to inoculate a 40 mL YEP-lactate culture (OD = 0.2) at 30°C. Alternatively, strains carrying *URA3*-containing multicopy plasmids for *TOP3* or *MUS81/MMS4* alleles overexpression (WDHY4618, 4619, 4620, 4696, 4697, 4698, 4783, 4784, 4785, and 4786) were, from a SD-URA pre-culture, diluted in Lactate-URA. When the cells entered log phase (OD ≈ 0.5-0.8), the basal Lys^+ frequency is determined by plating on SD–LYS and YPD plates (control plating) and the expression of the HO endonuclease is triggered in the remaining culture upon addition of 2% galactose. Two hours after, when HO cutting is > 99% (Figure 2B), the induced Lys^+ frequency is determined by plating again on SD–LYS and YPD plates. Basal and induced Lys^+ frequencies as well as viability (Figure S3A) are determined after incubation of the plates at 30°C for 2-3 days (or more in the case of slow growing mutants). In rare instances, an early clonal (jackpot) event in the starter colony yielded very high basal frequency, precluding determination of the induced frequency. These colonies were removed from the analysis, and consequently we did not systematically determine the basal Lys^+ frequency. A minimum of 3 independent experiments have been performed for each strain. Translocation frequencies are reported Table S3.

Translocation assay upon transformation of a linearized plasmid

An exponentially growing YPD culture of strains lacking the DSB-inducible construct and bearing either the inter-chromosomal donors or the intra-chromosomal donors (WDHY4436 and WDHY4948, respectively) were used for transformation. A total of 10^8 cells were transformed with either no DNA (control), or 140 fmol of pRS415 or 140 fmol of circular or *Xba*I-digested pWDH1082 (annotated sequence Data S1), using standard Lithium-Acetate-PEG heat-shock transformation protocol. *Xba*I linearizes the plasmid in place of the HO cut site, mimicking the integrated situation. The transforming plasmid thus has YS(2000-2000) construct at one extremity of the linearized fragment and 5,608 bp of heterologous backbone DNA at the other extremity. Cells transformed by pRS415 were plated on SD-LEU and YPD plates to determine the transformation efficiency (mean ± SD: $1.1x10^{-4} \pm 5.5x10^{-5}$, n = 14). Non-transformed cells and cells transformed with no DNA, circular pWDH1082, or *Xba*I-linearized pWDH1082 were plated on SD-LYS and YPD plates. The induced Lys^+ frequency was normalized by the transformation efficiency. No Lys^+ cells were recovered before transformation or by transformation in the absence of DNA or using circular pWDH1082. The co-transformation efficiency (mean ± SD: 11.6 ± 2%, n = 3) has been determined upon transformation of 140 fmol of both pRS415 (*LEU2*) and pRS327 (*LYS2*) upon plating onto SD-LEU, SD-LYS and SD-LEU-LYS plates.

Translocation assay in G1-arrested cells and FACS analysis

Several genetic modifications were required to perform the translocation assay upon induction of the DSB in the G1 phase of the cell cycle in a diploid strain. First, the strain is deleted for the *MAT*α copy and for the protease-encoding gene *BAR1* to allow for robust arrest in G1 upon α-factor treatment. Second, *KU70* was deleted to enable DNA resection and HR in G1 (Barlow et al., 2008). Early log-phase (OD ≈ 0.3) cultures of the resulting *bar1Δ ku70Δ MAT***a** hemizygous strain (WDHY5010) were incubated for 4 hr with 50 ng/mL α-factor (Sigma). Synchronization was verified by the presence of "schmoo" in the majority of cells. Basal level plating, galactose addition and induced plating were performed as described above. Samples were collected for FACS analysis before α-factor addition (asynchronous), at the time of basal level plating (G1-arrested, no DSB) and at the time of the induced plating (G1-arrested, DSB). Briefly, 10^7 cells were collected by centrifugation, re-suspended in 70% ethanol and fixed at 4°C with rotation for at least a week. Cells were re-suspended in 1 mL of 50 mM Sodium citrate pH 7.0, sonicated for 20 s on a Bioruptor, and re-suspended in 1 mL 50 mM sodium citrate pH 7.0 containing 0.25 mg/mL RNaseA. Following incubation at 50°C for 1 hr, cells were re-suspended in 1 mL of 50 mM sodium citrate pH 7.0 with 16 ug/mL propidium iodide. FACS profiles were determined on a FACScalibur and analyzed on Cyflogic 1.2.1.

Southern blot analysis of the translocants

Lys^+ colonies were patched on SD-LYS plates, and their DNA was extracted from a saturating overnight 5 mL SD-LYS liquid culture. To avoid clonal events, the basal Lys^+ colonies analyzed originate from independent starter colonies. DNA was digested by *Hind*III

(for the inter-chromosomal donor construct) or *Pst*I (for the ectopic and intra-chromosomal donor constructs) for 4 hr at 37°C and migrated overnight in 0.8% Agarose-LE (Affymetrix) in 1X TBE at 50 V. The DNA is transferred from the gel onto an Amersham Hybond-XL membrane (GE healthcare) following the manufacturer instructions (alkali protocol). The membrane was blocked with Church buffer (BSA 1%, Na_2HPO_4 pH7.3 0.25M, SDS 7%, EDTA 1mM) for 2-3 hr at 65°C. The LY, S2, or *LYS2* probes (2, 2, and 4 kb-long, respectively) together with Phage λ DNA (molecular ladder) were radio-labeled by random priming with P^{32}-αdCTP (6,000 Ci/mmol; Perkin-Elmer) using the Decaprime II kit (Ambion Inc) and incubated with the membrane overnight at 65°C. After 3 – 5 washes for 10 min at 65°C 20 mM (Na_2HPO_4 pH 7.3, 1% SDS, 1 mM EDTA), membranes were exposed for 8 to 24 hr, and the Storage Phosphor Screen (GE healthcare) scanned on a Storm Phosphorimager (Molecular Dynamics).

Time course analysis of DSB formation on chrV by Southern blot

Liquid cultures of WDHY5144 were performed as for the *LYS2* translocation assay, except that glucose (2% final) was added 2 hr after galactose addition, to match the plating situation on SD-LYS and YPD plates. For each time point, $2x10^8$ cells were harvested by centrifugation at 4°C, washed once in cold water, and frozen at −20°C. The purified DNA was digested with *Avr*II and Southern blot was performed as described above, with a 611 bp-long probe hybridizing the flanking region of the *URA3* gene (obtained by PCR with primers 5′-GCATCAATCCGTGTAAGCAG and 5′-CACATTAACCTTCTTTGATGGTC), a 592 bp-long loading control probe hybridizing the *RAD54* gene (obtained by PCR with primers 5′-GAAGGCCAAGAGTTCATCTTCC and 5′-CCCCGACGATCGAATTCTA), and Phage λ DNA (molecular ladder; phage λ DNA digested by *Hind*III/*Eco*RI). Quantifications were performed with ImageQuant 5.2 (Molecular Dynamics).

Analysis of DSB formation at the donors on chrII by pulse-field gel electrophoresis

Cells (5.10^8) were harvested by centrifugation at 4°C and washed three times in 20 mL of cold 50 mM EDTA pH 7.5. Cells were mixed at 40°C with 0.83% NuSieve Agarose (Lonza), 100 mM EDTA, 0.17 M Sorbitol, 17 mM Sodium Citrate, 1% β-mercaptoethanol, 0.1 mg/mL Zymolyase 100T (US Biological), distributed in CHEF plugs and let solidify in ice. Cells were spheroplasted and RNA digested 1h at 37°C with rotation in 5 mL of 10 mM Tris HCl pH 7.5, 450 mM EDTA, 7.5% β-mercaptoethanol, 10 mg/mL RNase A. The spheroplasting solution was replaced with 5 mL of a lysis solution (10 mM Tris HCl pH 7.5, 250 mM EDTA, 1% SDS, 1 mg/mL Proteinase K) and incubated O/N at 50°C. Plugs were stored at −20°C in storage buffer (50% Glycerol, 50 mM EDTA). Prior to migration, plugs were washed twice in 5 mL 0.5X TBE, and loaded in a 0.5X TBE, 1% Seakeam Gold agarose gel. The wells were sealed with 1% NuSieve agarose. The gel was run in 0.5X TBE for 24 hr on a CHEF Mapper system (Bio-Rad) with the following parameters: voltage $6V/cm^2$, 120° angle, initial switch time 60 s, final switch time 120 s with a linear ramp. The gel was transferred on a Hybond-XL membrane, crosslinked and hybridized as described above. The centromere-containing chrII fragment was revealed using a 1,533 bp-long probe against the *MMS4* locus (amplified with the primers oIWDH2033 5′-GCTGGTTGCTTGTGATAACTC-3′ and oIWDH2034 5′- AGCTTGATTGCACAACTGC-3′), located ≈40-kb away from the *LYS2* locus. The centromere-devoid chrII fragment was revealed using a 1700 bp-long probe against *MEC1* (amplified with the primers oIWDH2036 5′- GAACACCCTCATAAGAAACC-3′ and oIWDH2037 5′- GAAACTTTATCAGCGTGGC-3′). Membranes were stripped by incubating them twice for 30 min at 95°C in 100 mL of 1% SDS.

ChrII and V copy number analysis by quantitative PCR

Quantitative PCR was performed in duplicate in 96-well plates with the Roche SYBR Green I Master kit according to manufacturer instructions, and run on a Roche Light Cycler 480. Data were analyzed using the Light Cycler 480 Software 1.5.0. All signals were normalized to the homozygous *ARG4* control locus on chrVIII. The normalized signal of Lys^+ cells was then compared to the signal of the parental strain (determined in each 96-well plate) to estimate CNV (scheme Figure S5B for the allelic inter-chromosomal strain, and Figure S5E for the ectopic-*cis* strain). The sequence of the primers used for each loci is provided Table S2.

Multi-invasion-Capture assay

A wild-type (WDHY5325) and a *rad51Δ* (WDHY5147) strain were cultured up to exponential phase in YEP-lactate and DSB on Ch. V was induced as for the translocation assay. 10^8 cells were collected 3 hr post-DSB induction (or in the un-induced culture), pelleted and re-suspended in 2.5 mL of a Psoralen crosslinking solution (0.5 mg/mL Trioxsalen, 50 mM Tris HCl pH 8.0, 50 mM EDTA, 20% ethanol). Crosslink of cells was performed in a 60 mm petri dish upon UV irradiation (365 nm) in a Spectrolinker XL1500 (Spectroline) for 15 mn with circular agitation. Cells were washed in 50 mM Tris HCl pH 8 50 mM EDTA and the pellet stored at −20°C. Cells were spheroplasted in a zymolyase solution (0.4 M Sorbitol, 0.4 M KCl, 0.5 mM $MgCl_2$, 40 mM Sodium Phosphate buffer pH7.2, 20 μg/mL Zymolyase 100T (US Biological)) for 15 min at 30°C. Zymolyase was washed 3 times in spheroplasting buffer at 2,500 g and 3 times in Cutsmart Buffer 1X (NEB) at 16,000 g. Cells were resuspended in Cutsmart buffer 1.4 X at a final concentration of $2x10^8$ cells/mL and stored at −80°C. Chromatin of $2x10^7$ cells is solubilized upon incubation at 65°C for 10 min with 0.1% SDS, and SDS is quenched by addition of 1% Triton X-100. DNA is digested by 20 units of *Eco*RI-HF (NEB) at 37°C for 1 hr. Proteins are denatured by addition of 2% SDS and incubation at 55°C for 10 min. Cells are put in ice and SDS is quenched by addition of 6% Triton X-100. Ligation is performed in 800 uL of a ligation mix (50 mM Tris-HCl pH 8.0, 10 mM $MgCl_2$, 10 mM DTT, 1 mM ATP, 0.25 mg/mL BSA, 300 units of T4 DNA ligase (Bayou Biolabs)) at 16°C for 1h30. 25 μg/mL Proteinase K is added and proteins digested for 30 min at 65°C. DNA is extracted following a standard Phenol:Chloroform:Isoamyl Alcohol and isopropanol precipitation procedure. DNA pellets are re-suspended

and incubated at 30°C in 50 μL 10 mM Tris HCl pH 8.0, 1 mM EDTA, 0.4 mg/mL RNase A. The quantitative PCR was performed on a Roche LightCycler 480 machine using the SYBR Green I Master kit (Roche), according to the manufacturer instructions. After an initial denaturation phase, the cycling conditions were 95°C for 10,'' 66°C for 12,'' 72°C for 12,'' repeated 50 times. The nature of the amplified product was confirmed by a final thermal denaturation ramp. Four reactions were performed: a loading standard (*ARG4*) on which the other reactions are normalized; a control to verify DSB formation at HOcs on chrV; a control of *Eco*RI digestion and intra-molecular ligation efficiency on a 1,904 bp fragment at the *DAP2* locus; a reaction to detect the product of the ligation of the 5′ flanking regions of the LY and S2 donors. Data were analyzed using the Light Cycler 480 Software 1.5.0.

QUANTIFICATION AND STATISTICAL ANALYSIS

Translocation (Lys^+) frequencies were compared using the nonparametric Mann-Whitney-Wilcoxon unpaired test. For exact frequencies, SEM and number (n) of independent experiments performed, see Table S3. Proportions of rearrangements observed by Southern blot and qPCR have been compared using the Fisher's exact test. Statistical cutoff was set to $\alpha = 0.05$ for all tests. All statistical tests were performed under R x64 3.2.0.

DATA AND SOFTWARE AVAILABILITY

Construct sequences

The annotated sequences of the various DSB-inducible constructs, donor variants, and plasmids used in this study are available as *.ape (ApE Plasmid Editor) files in the Data S1: DNA construct sequences (Related to the STAR Methods).

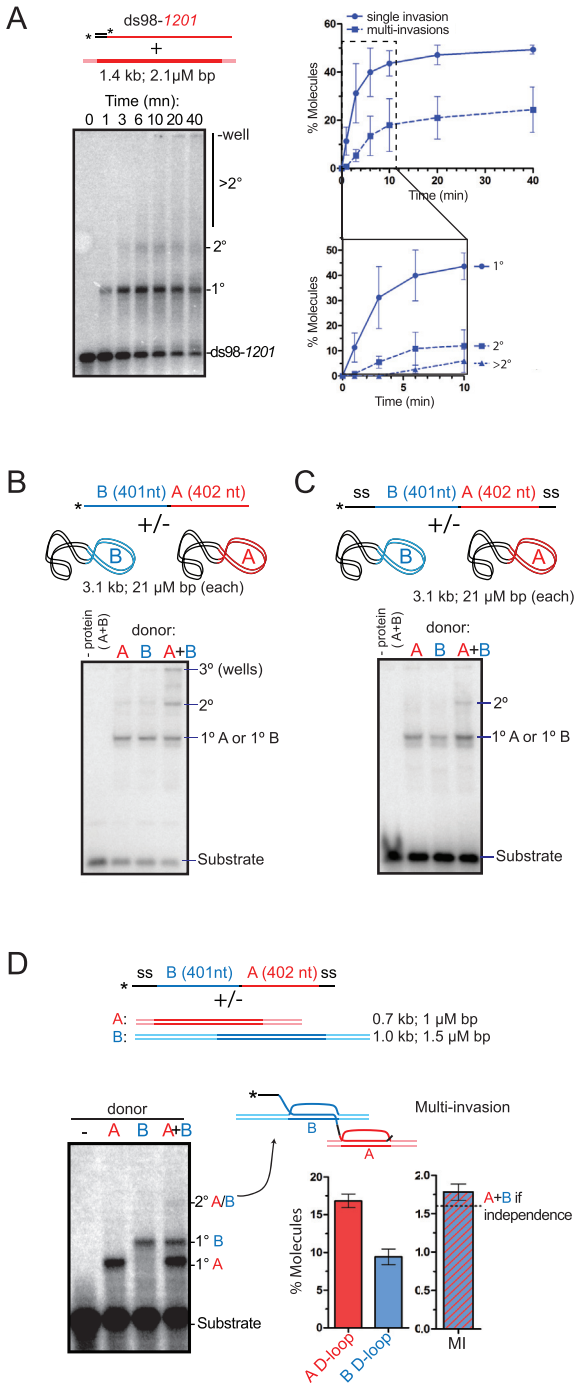

Figure S1. Long Rad51-ssDNA Filaments Form Multi-invasion on Linear dsDNA In Vitro, Related to Figure 1

(A) Time course analysis of single and multi-invasion of a linear dsDNA donor (1.5 nM molecules) by the *ds98-1201* substrate (0.5 nM molecules).
(B) D-loop reactions with chimeric ssDNA substrate (B401-A402, 1 nM molecules) sharing homology with two different sc DNA donors (A and B).
(C) Same as in (B) but using a chimeric substrate with heterologous 5′- and 3′ ends (ss141-B402-ss17-A402-ss78; 1 nM molecules).
(D) same as in (C) but using two linear dsDNA donors A and B bearing 5′- and 3- terminal heterologies of different length (100 and 200 bp for donor A and 400 and 200 bp for donor B; 1.5 nM molecules). Quantification of the A and B single invasions (left panel) as well as invasion of both A and B (MI, right panel) are shown. The expected amount of MI in case of independence of the A and B invasion events (1.6%) is the product of the two measured single invasions (17% and 9.2%).
(A–D) Reaction performed with yeast Rad51, Rad54, and RPA. (A and D) Quantifications show the mean and standard deviation of three independent experiments.

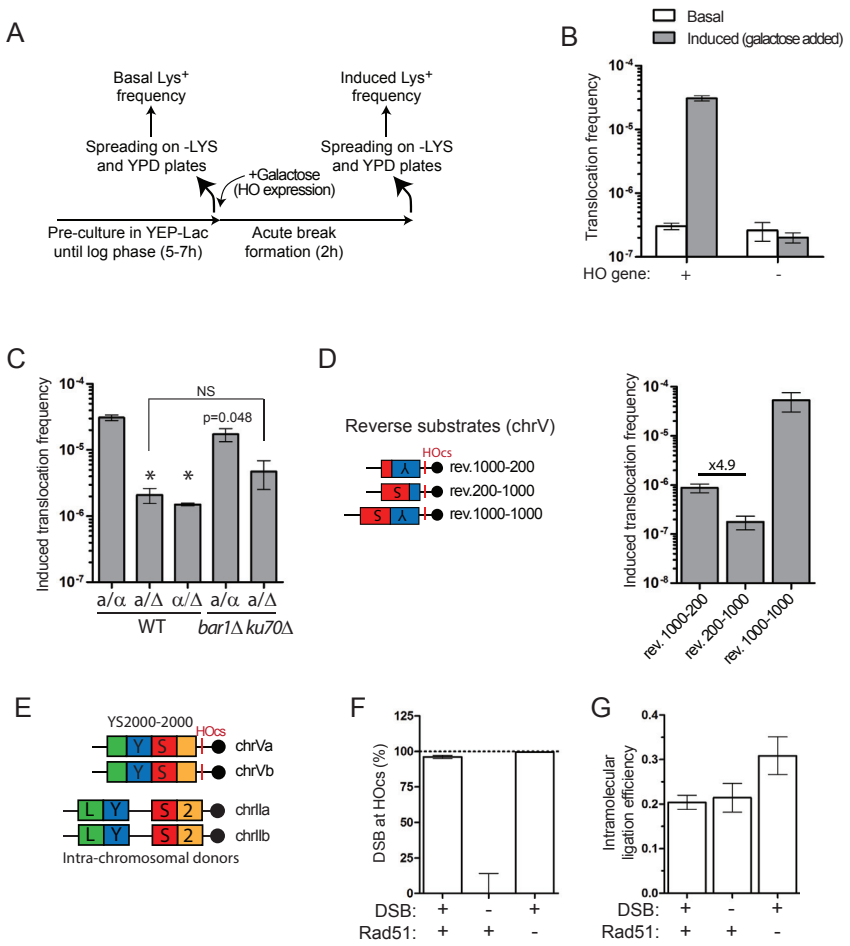

Figure S2. A Single Rad51-ssDNA Filament Invades and Causes Translocation of Two Intact Donors in *S. cerevisiae*, Related to Figures 2 and 3

(A) Experimental scheme.

(B) Translocation frequency in the reference inter-chromosomal strain bearing or not the GAL-HO expression construct. The basal translocation frequency is not significantly different between the two strains. Galactose addition do not cause a no significant increase of the translocation frequency in the strain lacking the inducible HO gene.

(C) Effect of *MAT* heterozygosity on the translocation frequency in wild-type and *bar1Δ ku70Δ* strains. * indicate significant differences ($p < 0.05$) compared to the wild-type strain. NS: not significant.

(D) Induced translocation frequency in strains with a reversed YS1000-1000, YS1000-200, or YS200-1000 DSB-inducible constructs.

(E) Schematic of the wild-type strain used to physically detect MI. The strain bears homozygous copies of both the LY and S2 donors in the *intra*–chromosomal configurations and an homozygous DSB-inducible construct (YS2000-2000).

(F) Control for DSB induction at HOcs. (G) Control for EcoRI digestion and intramolecular ligation efficiency.

(B, C, D, F, and G) Bars represent mean and SEM.

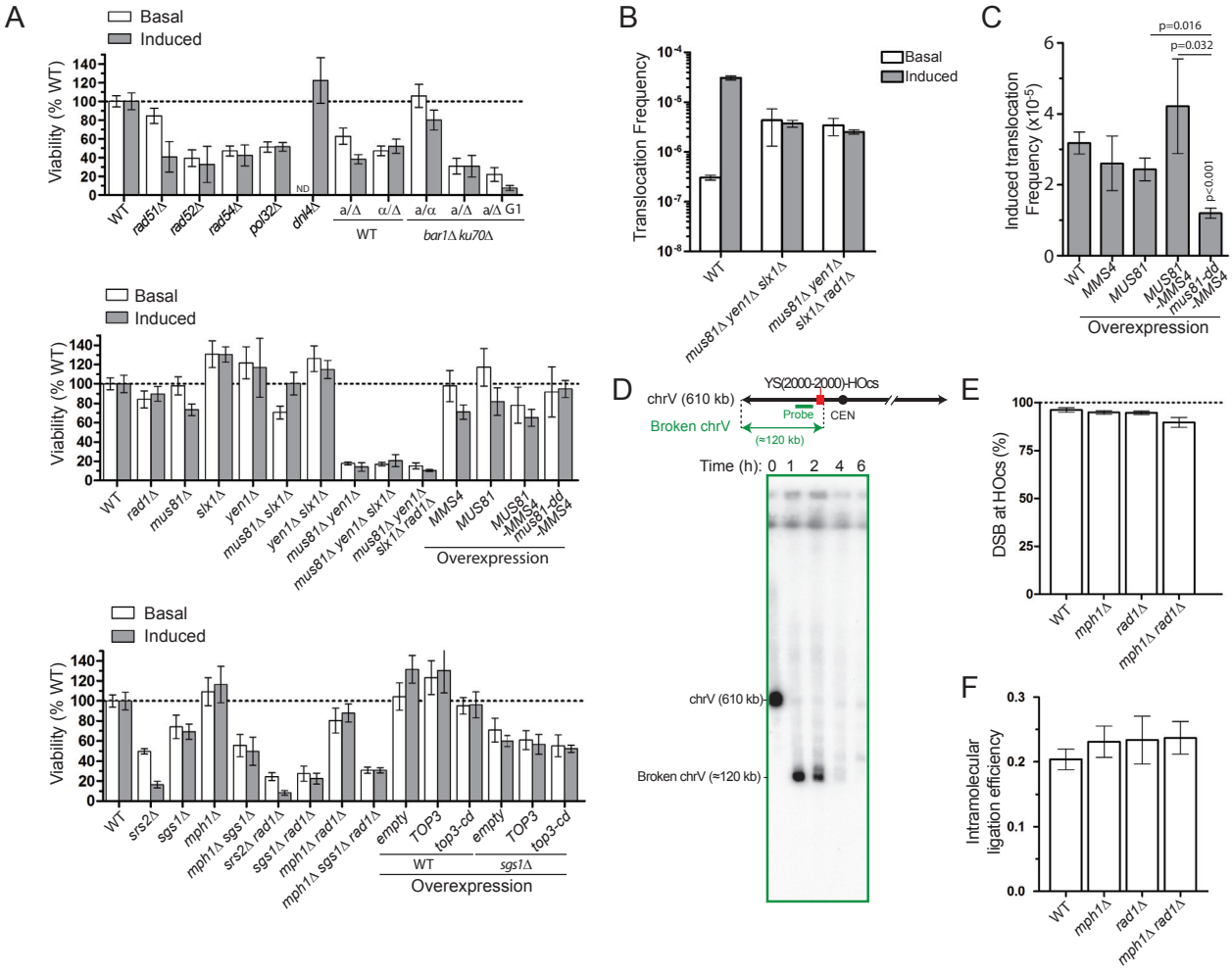

Figure S3. Genetic Control of MIR, Related to Figure 4

(A) Viability of mutant strains used in this study (expressed as a percentage of wild-type strain viability).

(B) No induction of the Lys$^+$ frequency upon DSB formation in the *mus81Δ yen1Δ slx1Δ* and *mus81Δ yen1Δ slx1Δ rad1Δ* strains.

(C) Induced Lys$^+$ frequencies in strains overexpressing *MMS4*, *MUS81*, both *MMS4* and *MUS81*, or both *MMS4* and the *mus81-dd* allele encoding a catalytic-deficient version of Mus81. Lys$^+$ frequencies were compared using a Mann-Withney unpaired test.

(D) Southern blot analysis of the DSB formation kinetics at HOcs on chrV. The probe hybridize the immediate unique region 5′ of the DSB-inducible YS2000-2000-HOcs contruct.

(E) Kinetics and genetic requirements of breakage at the donor site on chrII following DSB induction at HOcs on chrV.

(E and F) MI-Capture controls for DSB induction at HOcs (E) and for EcoRI digestion and intramolecular ligation efficiency (F) in the WT, *mph1*Δ, *rad1Δ*, and *mph1Δ rad1Δ* strains.

(A–C, E, and F) Bars represent mean and SEM.

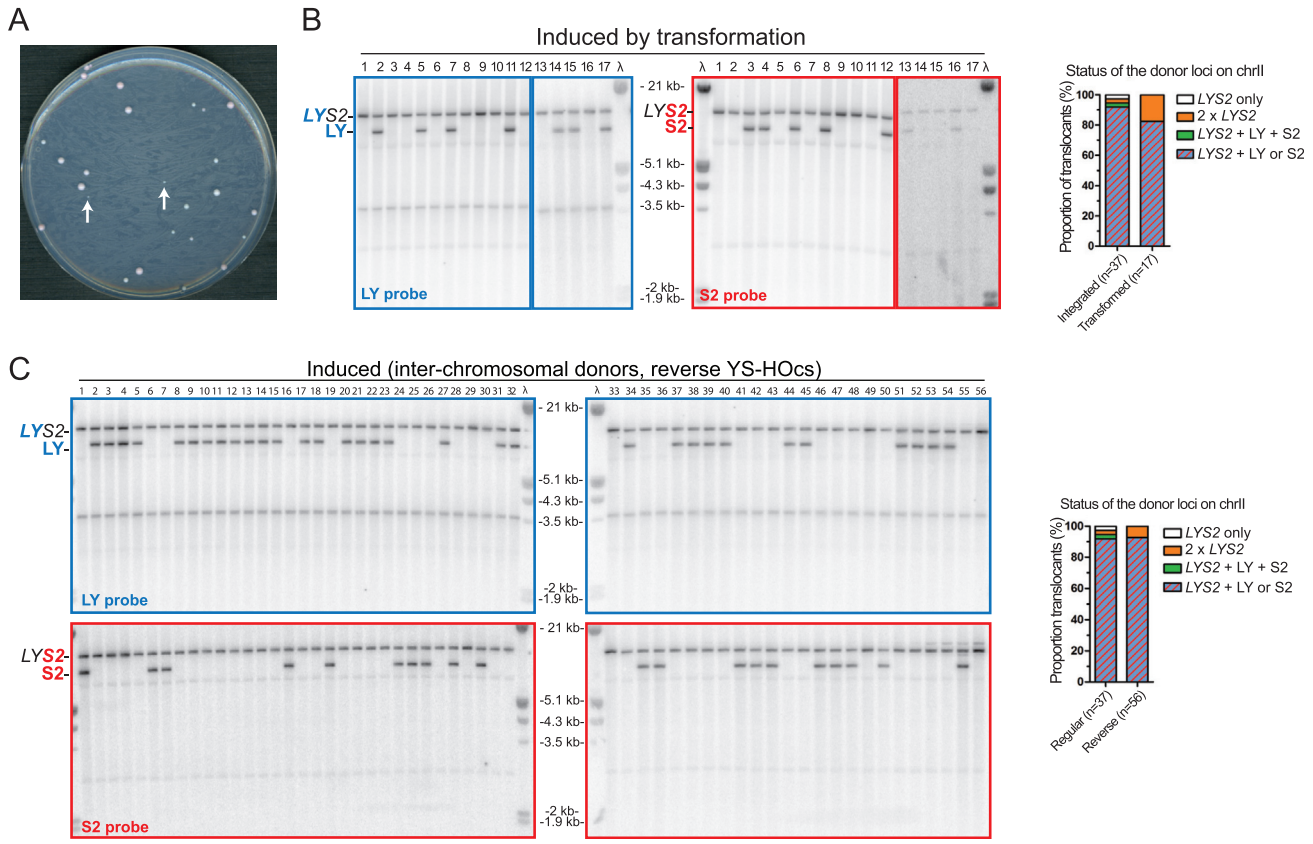

Figure S4. Physical Analysis of MIR Translocants, Related to Figure 5

(A) Representative SD-LYS plate showing the colony size heterogeneity upon plating induced wild-type cells. White arrows show colonies considered "small" in the analysis Figure 6.

(B) Southern blot analysis of 17 translocants induced in the transformation experiment (Figure 3B) in a strain bearing donors in the inter-chromosomal configuration but lacking the YS-HOcs DSB-inducible construct. The segregation pattern of *LYS2* and the donors is not significantly different from MIR events induced with the integrated YS-HOcs construct.

(C) Southern blot analysis of 56 induced translocants obtained in the wild-type strain bearing a reversed YS sequence near the HOcs (translocation frequency not significantly different from the regular orientation, Figure S2D). Summary of the donor and *LYS2* segregation pattern on chrII are shown on the right.

(B and C) The DNA was digested by *Hind*III as in Figure 5A. Other legend as in Figure 5A.

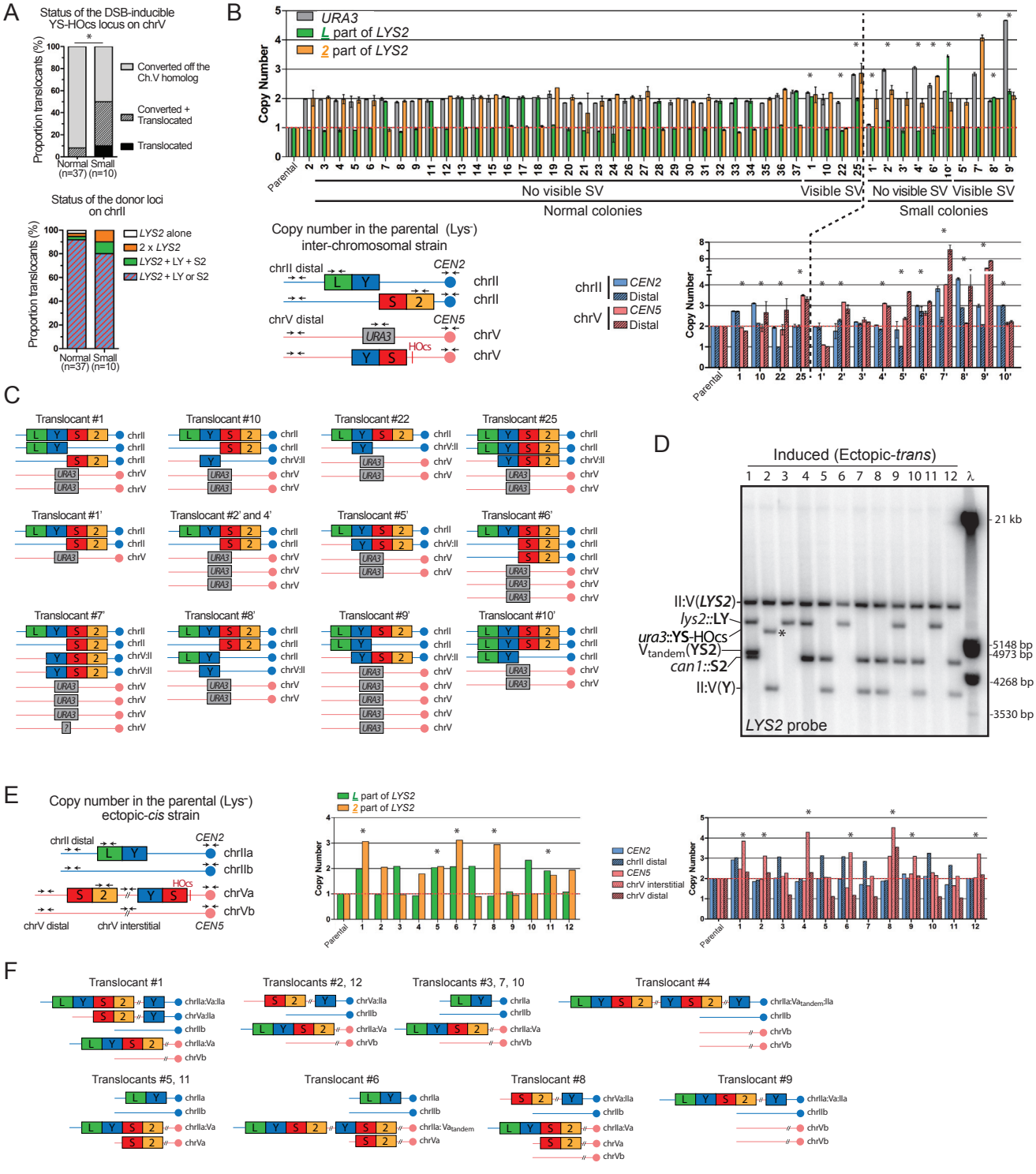

Figure S5. MIR Is Frequently Associated with Additional Chromosomal Abnormalities, Related to Figure 6

(A) Summary of the status of the DSB-inducible YS-HOcs construct (left) and the segregation pattern of the donors (right) in normal (n = 37) and small (n = 10) induced Lys$^+$ colonies obtained in the reference (inter-chromosomal) strain. *p < 0.05 (Fisher's exact test).

(B) Copy number analysis of multiple loci on chrII and V by quantitative PCR in the normal (n = 37) and small (n = 10) induced Lys$^+$ colonies analyzed by Southern blot in Figures 5A and 6A. * copy number abnormality.

(C) Summary of the genetic content of translocants exhibiting additional chromosomal abnormalities obtained in the inter-chromosomal donor configuration.

(legend continued on next page)

(D) Southern blot analysis of induced Lys$^+$ colonies (n = 12, normal colonies) obtained with the ectopic-*trans* donors strain. * band of unknown origin slightly smaller than the uncut *ura3*::YS-HOcs construct. Other legend as in Figure 6C.
(E) Copy number analysis of multiple loci on chrII and V by quantitative PCR in the induced ectopic-*cis* translocants analyzed by Southern blot in Figure 6C.
(F) Summary of the genetic content of the 12 ectopic-*cis* translocants deduced from Southern blot (Figure 6C) and qPCR analysis (Figure S5E).

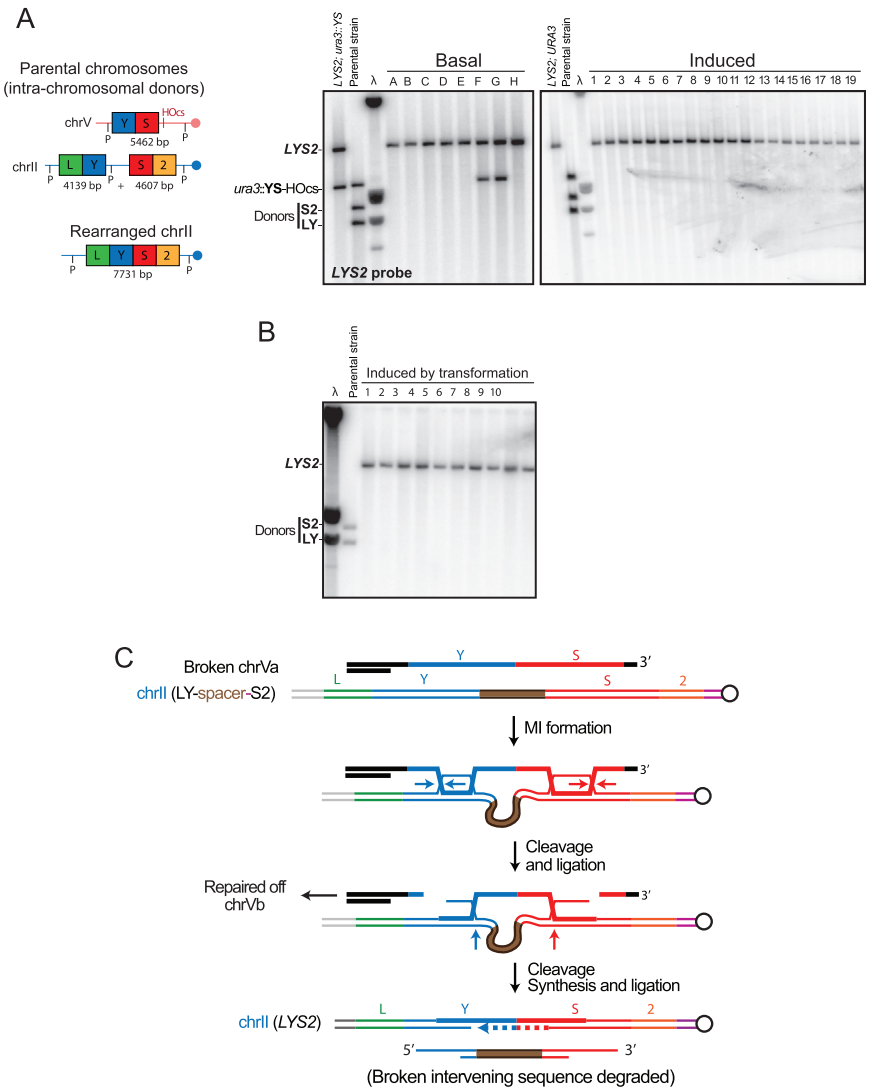

Figure S6. Physical Analysis of Translocants Obtained in the Intra-chromosomal Donor Configuration, Related to Figure 6

(A) Southern blot analysis of basal (n = 8) and induced (n = 19) translocants resulting from the intra-chromosomal donor configuration (Figure 3C). Expected fragments length upon PstI digestion is indicated. Other legends as in Figure 6C.

(B) Southern blot analysis of 10 translocation obtained in the transformation experiment (Figure 3B) of a strain bearing intra-chromosomal donors and lacking the integrated YS-HOcs construct.

(C) Model for MIR in the intra-chromosomal context, a variation on the theme of Mechanism 1 (Figure S7). Here, because the two single-ended DSBs are inflicted in close proximity (~1-kb) on the same molecule, exonucleolytic degradation will likely eliminate the intervening dsDNA and preclude formation of additional rearrangements.

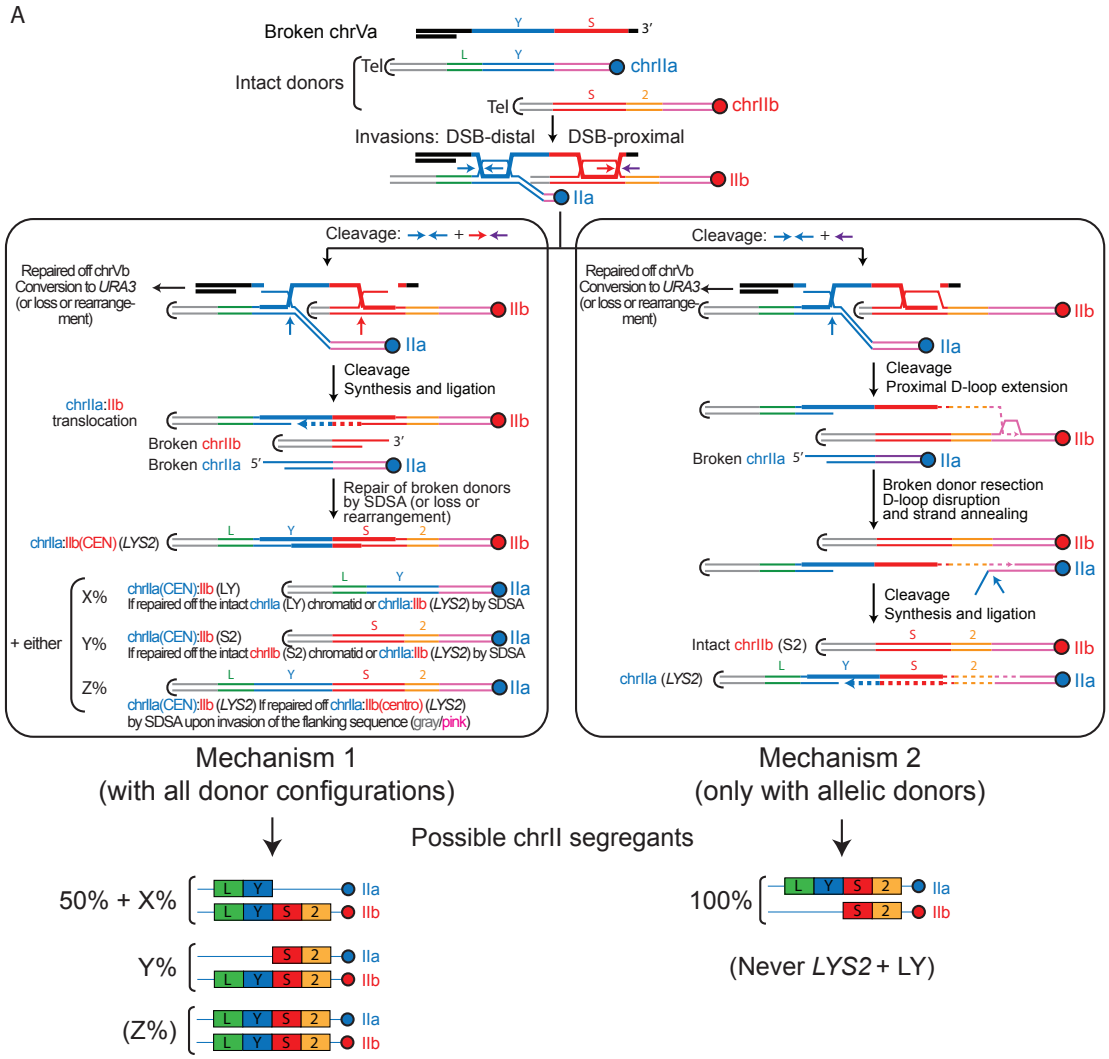

Figure S7. Putative MIR Mechanisms, Related to Figure 7

Both MIR mechanisms require endonucleolytic cleavage of the internal heteroduplex DNA junction, which allows for ligation of the 5′ side of the internal donor with the invading molecule. Similar endonucleolytic processing of DNA strand exchange intermediates in vivo were also proposed by others (Mazón and Symington, 2013; Pardo and Aguilera, 2012; Stafa et al., 2014) and have been demonstrated to occur in vitro (reviewed in Schwartz and Heyer, 2011). The converse endonucleolytic processing of the DSB-proximal invasion is specific to Mechanism 1 and allows for ligation of the invading molecule with the 3′ side of the DSB-proximal donor. These symmetrical cleavage-ligation steps in both hDNA region create a physical link between the two donor chromosomes bridged by the intervening sequence of the invading molecule. Gap filling using the invading molecule as a template completes the translocation process while inserting the intervening sequence between the two cleavage/ligation sites. As a consequence of the endonucleolytic processing of the DSB-proximal and internal invasions, Mechanism 1 leaves the left side of the internal donor with a 3′ protruding single-ended DSB and the right side of the donor with a 5′ protruding single-ended DSB. If MIR has translocated allelic donors (*e.g.* inter-chromosomal configuration), the flanking homologies of the donors enable repair of these oriented single-ended DSBs by SDSA off an intact chromatid (being either LY, S2, or the restored *LYS2*). Consequently, the *LYS2* translocation carried in place of the S2 donor (chrIIb) is expected to segregate with the intact chromatid of chrIIa (bearing an unbroken LY donor) in 50% of the cases, and with the outcome of the repair of the broken chromatid (LY, S2 or *LYS2*) in the remaining 50% of the cases. If MIR has translocated ectopically positioned donors (*e.g.* ectopic-*cis* and -*trans* configurations) repair by SDSA is impossible and the single-ended DSBs generate additional rearrangements (see Figure S8).

Contrary to Mechanism 1, Mechanism 2 exploits the DSB-proximal invasion as in the SDSA model, by reannealing the extended DSB-proximal extremity of the invading molecule onto the broken internal donor (LY). This extension step is the only envisionned displacement DNA synthesis in MIR. A gap filling mechanism similar to Mechanism 1 will complete the translocation process. The reannealing step of Mechanism 2 is possible only if the internal and DSB-proximal donors share flanking homologies (e.g., in the allelic inter-chromosomal configuration), thus restraining Mechanism 2 to specific sequence contexts. Notably, Mechanism 2 do not propagate additional single-ended DSBs, and causes the *LYS2* translocation to be carried in place of the LY donor (chrIIa). Consequently, 100% of the *LYS2* translocation is expected to segregate with the S2 donor (chrIIb).

In summary, Mechanism 1 causes the translocation to be carried in place of the DSB-proximal donor (e.g., S2) and propagate two single-ended DSBs onto the donors, while Mechanism 2 causes the translocation to be carried in place of the internal (e.g., LY) donor and do not propagate additional DSB. Hence, the contribution of each mechanism can be deduced from the segregation profile of the translocation with the intact LY and S2 donors (Figure 5E). The fact that more

(legend continued on next page)

than half, but not 100% of the translocation segregate with the S2 donor indicates that both mechanisms are at play in the allelic reference strain. Based on the proportion of LY and S2 segregation (Figure 5E) and extreme scenarios where the repair outcome of the single-ended DSBs in Mechanism 1 restores LY (X%) range from 50 or 0%, we estimate that Mechanism 1 accounts for ≈30 – 60% of MIR events in an allelic donor configuration.

Contrary to Mechanism 2, Mechanism 1 applies to all sequence contexts and poses the additional threat of propagating two single-ended DSBs. This break cascade has the potential to triggering additional local rearrangements (Figure S8) in a manner dependent on the surrounding sequence context. This differential opportunity for accurate repair explains the higher proportion of additional SV and CNV associated with the MIR translocation in the ectopic versus the allelic donor contexts (Figure 6D).

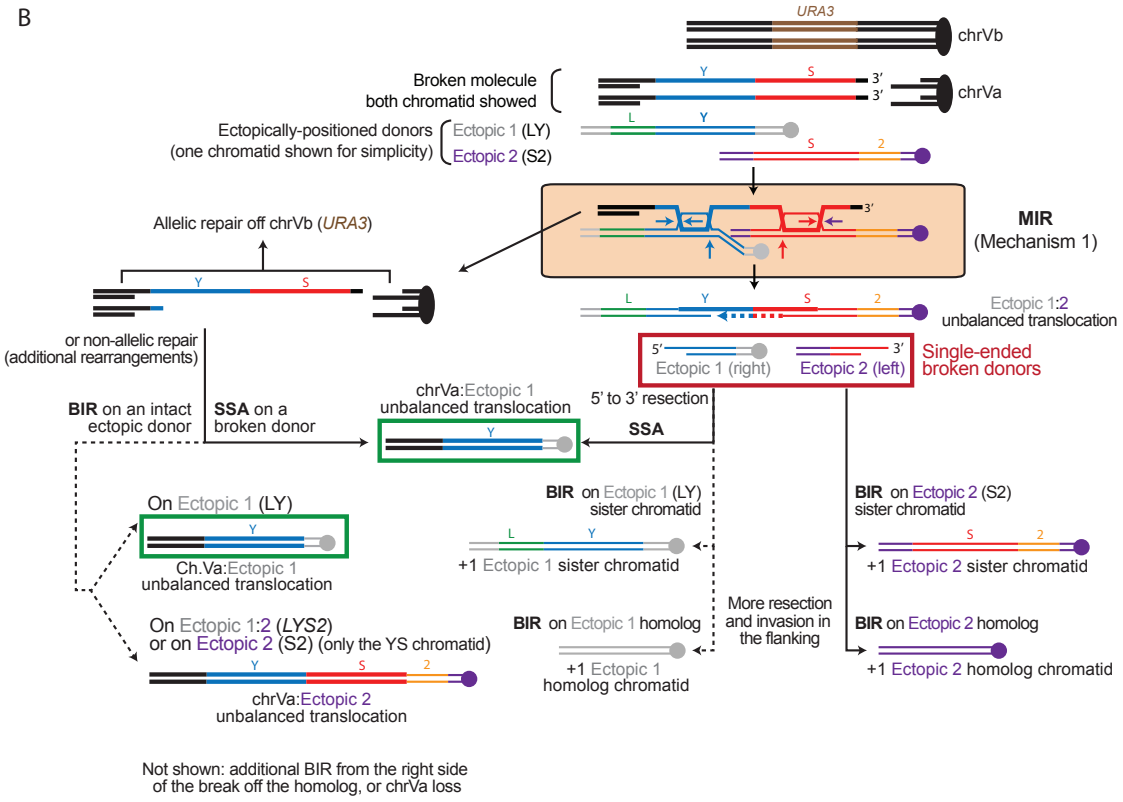

Figure S8. Proposed Mechanisms for the Formation of MIR-Associated Additional Rearrangements, Related to Figure 7

Proposed mechanisms for the formation of MIR-associated additional rearrangements in the ectopic donor configurations. In this context, all the MIR events are generated by Mechanism 1, which produce two single-ended DSBs that cannot be repaired by SDSA. The most prevalent rearrangement observed is a chrV:II unbalanced translocation leaving the "Y" part of *LYS2* at the junction (50% cases, Figures 6C and S5F), exclusive with the presence of the intact donor. This translocation can be straightforwardly explained by SSA of the broken LY donor and a resected YS chromatid (boxed in green). The less frequently observed chrV:II (YS2) translocation can be explained by a BIR event or half-crossover initiated by the originally broken YS molecule onto the S2 donor. Repair of the S2 donor is only possible by BIR, generating a supplementary chrV chromatid that has a 50% chance to segregate with *LYS2*, consistent with the proportions determined for both the ectopic-*cis* and ectopic–*trans* strains.